ACS APPLIED MATERIALS & INTERFACES

www.acsami.org

Research Article

Metal–Organic Framework Induced Stabilization of Proteins in Polymeric Nanoparticles

Md Rakib Hasan Khan,[#] Zoe Armstrong,[#] Mary Lenertz, Briana Saenz, Narendra Kale, Qiaobin Li, Austin MacRae, Zhongyu Yang, and Mohiuddin Quadir*

Cite This: *ACS Appl. Mater. Interfaces* 2024, 16, 14405–14420

Read Online

ACCESS | Metrics & More | Article Recommendations | Supporting Information

ABSTRACT: Developing protein confinement platforms is an attractive research area that not only promotes protein delivery but also can result in artificial environment mimicking of the cellular one, impacting both the controlled release of proteins and the fundamental protein biophysics. Polymeric nanoparticles (PNPs) are attractive platforms to confine proteins due to their superior biocompatibility, low cytotoxicity, and controllable release under external stimuli. However, loading proteins into PNPs can be challenging due to the potential protein structural perturbation upon contacting the interior of PNPs. In this work, we developed a novel approach to encapsulate proteins in PNPs with the assistance of the zeolitic imidazolate framework (ZIF). Here, ZIF offers an additional protection layer to the target protein by forming the protein@ZIF composite via aqueous-phase cocrystallization. We demonstrated our platform using a model protein, lysozyme, and a widely studied PNP composed of poly(ethylene glycol)-poly(lactic-*co*-glycolic acid) (PEG–PLGA). A comprehensive study via standard loading and release tests as well as various spectroscopic techniques was carried out on lysozyme loaded onto PEG–PLGA with and without ZIF protection. As compared with the direct protein encapsulation, an additional layer with ZIF prior to loading offered enhanced loading capacity, reduced leaching, especially in the initial stage, led to slower release kinetics, and reduced secondary structural perturbation. Meanwhile, the function, cytotoxicity, and cellular uptake of proteins encapsulated within the ZIF-bound systems are decent. Our results demonstrated the use of ZIF in assisting in protein encapsulation in PNPs and established the basis for developing more sophisticated protein encapsulation platforms using a combination of materials of diverse molecular architectures and disciplines. As such, we anticipate that the protein-encapsulated ZIF systems will serve as future polymer protein confinement and delivery platforms for both fundamental biophysics and biochemistry research and biomedical applications where protein delivery is needed to support therapeutics and/or nutrients.

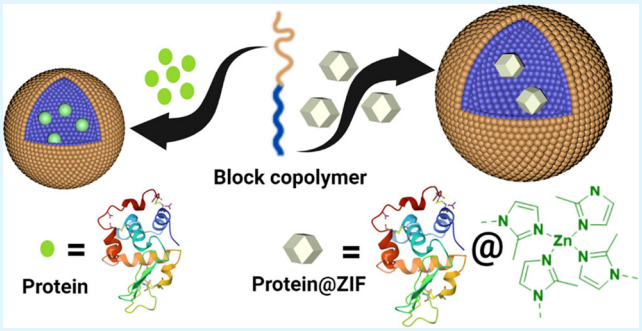

KEYWORDS: *polymeric nanoparticles, lysozyme, protein delivery, metal–organic framework (MOF), zeolitic imidazolate framework (ZIF), encapsulation*

1. INTRODUCTION

Proteins play essential roles in biocatalysis, cellular structure, muscle motion, signaling/messaging, and immune systems in living organisms.[1−3] Extensive research efforts have been carried out to understand how proteins function in their physiological conditions and to develop proper delivery platforms to treat deficiency in certain proteins (as unencapsulated proteins would be destabilized or removed by the human immune system). However, both areas face challenges. First, most proteins are studied in dilute solutions, different from the highly crowded and confined physiological environment; the complexities in cellular components limit the direct in-cell study of proteins, leaving mimicking the best option to understand proteins. Also, although extensively developed, the direct application of the current platforms for protein delivery is challenged by structural disturbances to the target protein, poor loading capacity, and/or uncontrolled release from the encapsulating platform.

Protein delivery systems have various applications in biological research and therapeutics. They can be applied to enhance the therapeutic enzymes' effectiveness and selectivity, enabling the treatment of human illnesses and detoxification.[4] The application of protein delivery systems in targeted drug delivery enables the encapsulation and distribution of medications to certain body locations, increasing drug

Received: November 4, 2023
Revised: February 22, 2024
Accepted: February 28, 2024
Published: March 15, 2024

bioavailability and lowering systemic toxicity. Anticancer proteins and medications can be delivered straight to tumor cells via protein delivery systems, increasing therapy effectiveness and reducing adverse effects. Nanoparticle-encapsulated proteins can be utilized as contrast substances in imaging procedures so that particular tissues or disease indicators can be monitored. Additionally, protein delivery systems are essential for gene therapy because they can be utilized to transfer therapeutic genes to target cells, allowing for the modification of cellular processes or the treatment of genetic abnormalities. Moreover, growth factors and other bioactive proteins are delivered by protein delivery systems in tissue engineering to support tissue regeneration and repair.[5]

To mimic the cellular conditions, especially the confinement effects (as crowding effects can be conveniently mimicked via molecular crowder mixing), it is necessary to develop proper compartment materials. Meanwhile, if such materials are developed, they may also be the optimal vehicles to host and deliver proteins analogous to a situation of "one stone, two birds". Thus far, inorganic porous materials have been the most common choices for protein confinement,[6−10] yet proteins confined therein may suffer from chemical and mechanical stress, disrupting the protein's biological and structural integrity;[11] the potential cytotoxicity of the confinement-providing materials could also be a concern. Polymeric nanoparticles (PNPs) may reduce chemical and mechanical stress due to the intrinsic flexibility of polymers while offering a condition in the simultaneous presence of crowding and confinement effects; if properly chosen, polymeric nanoparticles may also improve protein stability, controlled release, and cellular uptake performance, enhancing the efficiency of protein delivery.[12,13]

Loading proteins into polymeric nanoparticles, however, is nontrivial. Traditionally, these nanoparticles, particularly derived from block copolymers, are frequently employed for drug delivery.[14] For our study, we selected poly(ethylene glycol)-*block*-poly(lactic-*co*-glycolic acid) (PEG−PLGA) as a representative block copolymer that self-assembles in the form of micelles or polymersome-type nanoparticles, depending on relative block lengths. The reason for our selection is, this class of polymers is widely used to develop translational therapeutic modalities, mostly because of their biocompatibility and biodegradability.[15,16] Diversified methods have been adopted to drive the self-assembly of PEG−PLGA into nanoparticles, mediated via noncovalent interactions, including but not limited to van der Waal's attraction, hydrophilic/hydrophobic interaction, coordinate bonds, ion-pairing interactions, and hydrogen bonding. During the self-assembly in an aqueous environment, the PEG block of the PEG−PLGA block copolymer constitutes the outer hydrophilic compartment and the PLGA block constitutes the inner hydrophobic core of the resulting nanoparticles. So far as systemic application is concerned, the PEG layer reduces nanoparticle opsonization and extends the systemic residence time of the particles in the body by forming a steric and stealth barrier around the particles. The hydrophobic core, on the other hand, can harbor many water-insoluble therapeutic compounds, thereby improving drug dispersibility/solubility in an aqueous environment.[17] An effective way to create block copolymeric nanoparticles is nonsolvent-induced phase separation, popularly known as "nanoprecipitation".[18] In this approach, the copolymer is dissolved in a solvent that solubilizes both blocks and eventually added to a second solvent that has diminished solubility for one of the individual blocks.[19,20] The nanoprecipitation method is a user-friendly method of preparing block copolymeric nanoparticles due to its quick processing times, minimal raw material requirements, and low energy cost.[21,22] Numerous reports have illustrated the utilization of this approach to load protein and drugs inside of polymeric nanoparticles.[23−26] When the method is applied for protein encapsulation, the loading of an organic-solvent-sensitive protein (usually suspended in the aqueous phase) into the polymeric nanoparticles relies on the random formation of hydrophobic cores. As such, the loading capacity of proteins inside nanoparticles prepared via the nanoprecipitation method might be relatively uncontrollable and possibly poor. Also, there is no control on the location of the encapsulated proteins; if a protein is "wrapped up" in the hydrophobic portion of the nanoparticles, then functional loss in proteins may occur. Lastly, undesired protein leaching could occur from these block copolymeric nanoparticles.

A possible solution is to add another layer of protection to the protein, which disassembles under certain external stimuli (to enable protein release). Metal−organic frameworks (MOFs)[27−30] can be an optimal secondary layer, especially those that can be formed via aqueous-phase cocrystallization (with proteins) and are sensitive to external stimuli (i.e., pH), such as the zeolitic imidazolate frameworks (ZIFs).[31] Zinc is the second-most-prevalent transition metal, and the imidazole group resembles a crucial component of histidine, making ZIFs biocompatible.[32] Furthermore, protein@ZIF biocomposites can be formed in water via one-pot coprecipitation regardless of the choice of the protein, making this strategy generalizable.[33] Lastly, ZIFs can be disassembled under weakly acidic pHs, which provides the opportunity to render the platform sensitive to low pH, a hallmark of microenvironmental conditions of many diseases, including cancer. Therefore, the proposed system has several advantages; the nanoparticles are formed by the nanoprecipitation method, which is a one-step method and hence requires a short preparation time along with a small amount of materials and consumes low energy.[21] Conversely, other methods in the literature, such as emulsion diffusion methods, emulsion-evaporation, and precipitation by salting-out, require an earlier emulsion, making the process more intricate and time-consuming.[18] Introducing the additional MOF layer to the protein significantly protects the protein from rapid disintegration. In contrast to traditional porous materials, MOFs have a remarkably high loading capacity for proteins because of their large pore size, tunable pore structure, and high surface area.[34] Additionally, the proposed system is pH-sensitive as our MOFs (ZIFs) can decompose under an acidic environment, making the protein delivery system stimuli-responsive.[31] Thus, MOFs can serve as multifunctional platforms for protein delivery. The literature showed that proteins can be immobilized onto MOFs by the successful adsorption of protein molecules into presynthesized MOFs.[33,35] Protein immobilization on biocompatible solid substrates is a good way to increase the stability and functionality of the protein. In addition to producing a strong enzyme structure and offering an ideal milieu for substrate mass transfer, a proper immobilization may fully preserve the biocatalytic properties of the protein.[36,37] Metal−organic frameworks (MOFs) are a large class of porous materials having the advantages of high surface area, porosity, structural variety, and flexibility to be modified with specific functions.[38] Because of their easily adjustable pore size and topology,

https://doi.org/10.1021/acsami.3c16534
ACS Appl. Mater. Interfaces 2024, 16, 14405−14420

MOFs have the potential to be a platform for the immobilization of a protein. Additionally, proteins have improved stabilities against a range of perturbation circumstances due to the strong interaction between them and the MOFs. Hence, enzyme immobilization has found its perfect platform in zeolitic imidazolate frameworks (ZIFs), a kind of MOF with porous materials reticularly composed of organic ligands and metal nodes connected by strong interactions.[39] Because of these attractive features, MOFs have a lot of biological potential applications in imaging, sensing, gas separation, drug and protein delivery, and catalysis.[36] It is important to know the interfacial compatibility between the MOF and the polymer to realize the full potential of the proposed MOF-encapsulated polymer system. As PEG−PLGA is a flexible polymer because its internal rotational degree of freedom is large enough, it exhibits an enhanced contact surface and hence improved adaptation of its structure to the MOF surface. Thereby, the irregularities at the MOF surface can be covered by PEG−PLGA. Even some penetration of the terminal groups of the polymer into the pores of the MOF can be observed.[40] It is even possible to see some polymer terminal groups penetrating the MOF's pores, which indicates the strong affinity between the MOF and the PEG−PLGA polymer. Thus, the encapsulated protein inside the MOF can be well-protected from the outside environment. Here, we employ ZIF and a model protein, lysozyme, to demonstrate ZIF-enabled protein loading inside polymeric nanoparticles composed of PEG−PLGA. Lysozyme's structure−function relationship has been widely studied.[41] To evaluate the effectiveness of ZIF in assisting protein loading within the nanoparticles, we compared the loading parameters, i.e., content, efficiency, structure, and function, of the encapsulated protein loaded inside the nanoparticles with or without encapsulating a priori inside ZIFs (Scheme 1). For this purpose, we created PEG−PLGA nanoparticles (PP) loaded with either lysozyme (L) or ZIF-lysozyme composite (lysozyme@ZIF) to develop our testing platform PP-L or PP-ZL, respectively. In details, the loading capacity, protein structural and dynamic alteration upon encapsulation, protein release profile, biological function, cytotoxicity, and cellular uptake were assessed and compared for each approach. We found that ZIF-encapsulation enhanced the protein loading and reduced the structural perturbation of the protein without compromising bioactivity and biocompatibility. This work represents the first report confirming the effectiveness of ZIF as a protection layer for protein encapsulation into block copolymeric nanoparticles via nanoprecipitation techniques. The results are impactful for guiding the rational design of more advanced MOF/ZIF-polymeric nanoparticle-based protein confinement and delivery platforms.

Scheme 1. Schematic Illustration of ZIF-Mediated Encapsulation of a Model Protein, Lysozyme, Inside PEG−PLGA Nanoparticles[a]

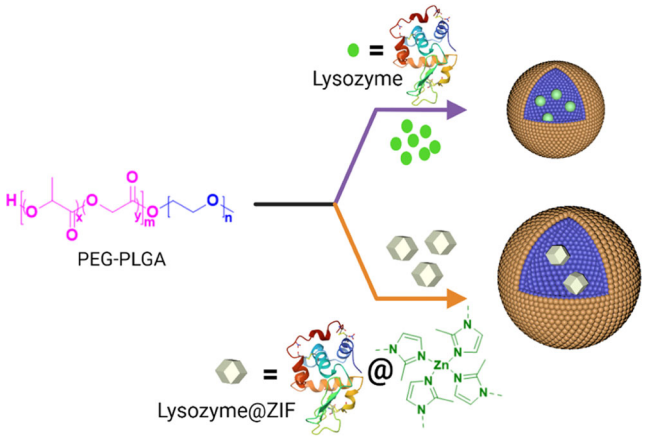

[a]Illustration of direct protein encapsulation in PEG−PLGA nanoparticles following the conventional nanoprecipitation method shown in the top part and ZIF-protected protein encapsulation in PP shown in the bottom part of the schematic. Object sizes are not scaled.

2. EXPERIMENTAL SECTION

2.1. Materials. Lysozyme from chicken egg white, poly(ethylene glycol) methyl ether-*block*-poly(lactide-*co*-glycolide) (mPEG-*b*-PLGA), dimethyl sulfoxide (DMSO), chemicals involved in ZIF preparation, bicinchoninic acid (BCA) assay kit, and *Micrococcus lysodeikticus* cells were purchased from Sigma-Aldrich. The chicken lysozyme enzyme-linked immunosorbent assay (ELISA) kit was purchased from Novus Biosystem. For evaluating nanoparticle cytotoxicity, L929 mouse fibroblast cells were used. For nanoparticle uptake studies, human pancreatic cancer cell line, BxPC3, was used. Both of these cell lines were procured from the American Type Culture Collection (ATCC, Manassas, VA).

2.2. Preparation of Lysozyme and Lysozyme@ZIF-Encapsulated Nanoparticles. The method used to prepare protein-encapsulated nanoparticles with or without ZIFs is illustrated in Figure 1. A nonsolvent-induced phase separation was adopted to prepare the protein-encapsulated nanoparticles.[42,43] PEG−PLGA is an amphiphilic block copolymer. It has both the hydrophilic domain (PEG) and the hydrophobic domain (PLGA) within the same matrix scaffold. In the nonsolvent-induced phase separation method, PEG−PLGA is dissolved in an organic solvent to form a homogeneous solution. Then, a nonsolvent that does not dissolve the polymer is introduced in the polymeric solution. In the presence of a nonsolvent, these block copolymers organize via self-assembly as a bilayer membrane, which eventually collapses into a spherical, hollow sphere entrapping the aqueous core.[44] This resulted in the formation of the PEG−PLGA biocomposite nanoparticles. While the PEG domain protected the nanoparticles from Ostwald ripening and acted against the Laplace pressure differentials, the interfacial tension and miscibility difference among the polymer-enriched phase, the solvent environment, and the nonsolvent environment essentially determined the particle size. As a suitable, nonselective solvent that dissolves both the blocks of the PEG−PLGA copolymer, DMSO was used. This solution was added to an aqueous solution of lysozyme (1 mg/mL), which served as the selective solvent for the PEG block of the copolymer at ambient temperature with moderate magnetic stirring. Under this condition, and in the presence of a lysozyme, the self-assembly process of the PEG−PLGA block copolymer led to the formation of protein-encapsulated nanoparticles.[45]

We were concerned that DMSO might disrupt the conformation of lysozymes encapsulated via this process. Electron paramagnetic resonance (EPR) spectroscopy showed that the lysozyme structure was not perturbed when the DMSO solution of the PEG−PLGA copolymer was added to the aqueous solution of the lysozyme. In order to purify the inhomogeneous nanoparticles and collect the targeted nanoparticles, centrifugation was performed as an initial step after the dialysis at 10,000 rpm for 10 min at 4 °C. This purification removed the inhomogeneous nanoparticles along with the unencapsulated lysozymes. However, after this step, there were still inhomogeneous particles present in the solution (Figure 2E); thus, the second step of purification needs to be performed, which is purification by filtration. Based on the targeted size of nanoparticles, syringe filters must be chosen. Nanoparticles with the desired size can be obtained through this two-step purification. Details of the preparative methods (solution concentration, reaction temperature,

https://doi.org/10.1021/acsami.3c16534
ACS Appl. Mater. Interfaces 2024, 16, 14405−14420

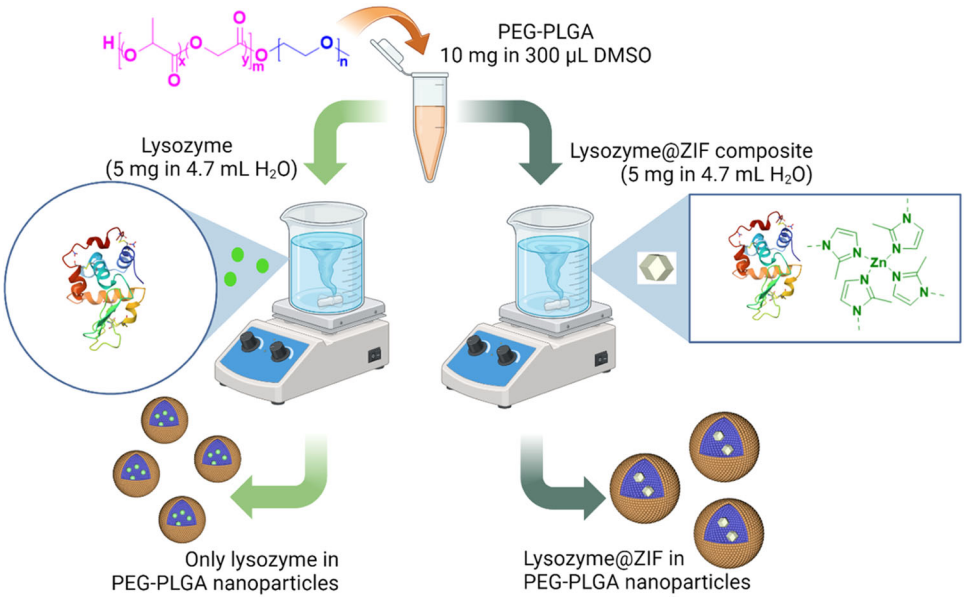

Figure 1. Steps toward the preparation of lysozyme-encapsulated PEG−PLGA nanoparticles. For lysozyme@ZIF biocomposites, instead of lysozyme alone, lysozyme@ZIF biocomposites were dispersed in deionized water (details are in the Supporting Information).

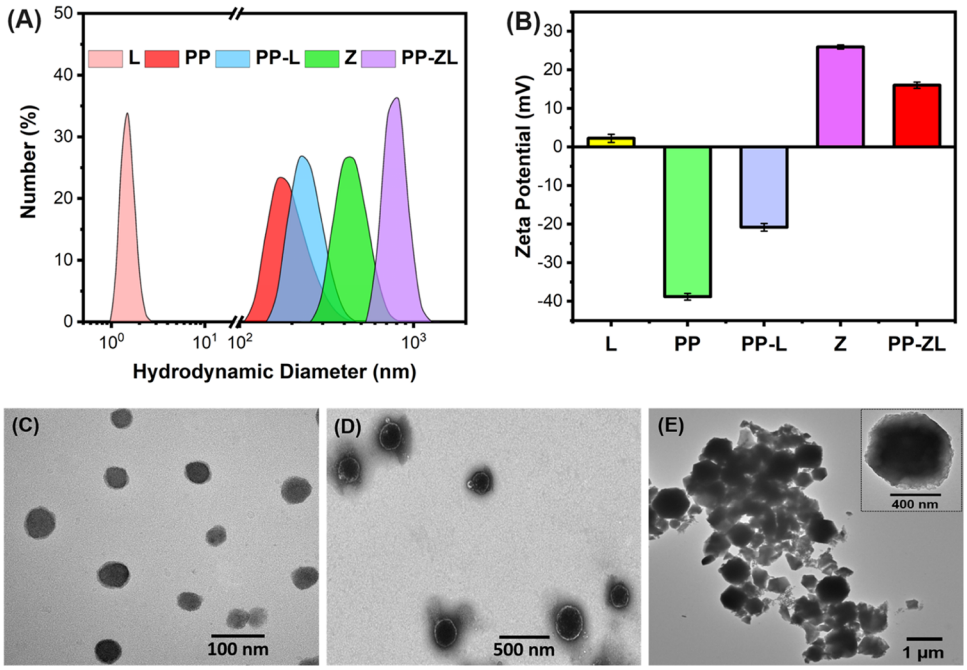

Figure 2. Nanoscale features of lysozymes encapsulated within PEG−PLGA systems. (A) Size measurement shows ZIF-associated systems are larger than the PEG−PLGA system. (B) ζ-potential study shows PP and PP-L systems demonstrate negatively charged ζ-potential, which reverses upon encapsulation of ZIF or lysozyme@ZIF. Error bars represent the standard deviation of the average of three separate measurements (N = 3). (C) TEM image shows a homogeneous distribution of PEG−PLGA nanoparticles. (D) Lysozyme-encapsulated PEG−PLGA nanoparticles (PP-L) show diameters larger than the PEG−PLGA systems (PP). (E) PEG−PLGA (PP)-bound lysozyme@ZIF biocomposites demonstrate a hexagonal structure of ZIF inside oval PEG−PLGA nanoparticles within a particle larger than other colloidal species used in this experiment.

and time) have been provided in the Supporting Information (SI). To prepare the lysozyme@ZIF biocomposites (ZL), we first encapsulated lysozymes in ZIFs, followed by dispersing the resultant lysozyme@ZIF biocomposites thoroughly in deionized (DI) water before the phase separation step via a high-speed vortex mixer, as detailed in the literature.[46] The resultant ZIF-bound lysozyme was dispersed in water at a lysozyme concentration of 1 mg/mL. Nanoprecipitation of the PEG−PLGA block copolymer dissolved in DMSO into this aqueous dispersion of ZIF-bound lysozyme resulted in the formation of ZIF-lysozyme-encapsulated PEG−PLGA systems. Table 1 shows the quantity of lysozyme loaded in the samples and the formula of each involved sample.

2.3. Nanoscale Characterization of Lysozyme-Encapsulated Nanoparticles. The particle size distributions were determined by dynamic light scattering (DLS),[47,48] while surface charges were evaluated using Doppler electrophoresis via a ζ-potential measurement. All measurements were performed in triplicate. The morphology of the involved nanoparticles was observed by using transmission electron microscopy (TEM) on samples suspended in phosphate buffer. Samples were dried and kept under a vacuum in a

https://doi.org/10.1021/acsami.3c16534
ACS Appl. Mater. Interfaces 2024, 16, 14405−14420

Table 1. Composition of Different Formulations Investigated in This Study

formulation[a]	lysozyme concentration (mg/mL)	copolymer concentration (mg/mL)	ZIF concentration (mg/mL)
L	1	0	0
PP	0	2	0
PP-L	1	2	0
Z	0	0	4
PP-ZL	1	2	4

[a]L = lysozyme; PP = PEG−PLGA nanoparticles; PP-L = lysozyme-loaded PP; Z = ZIF; PP-ZL = lysozyme@ZIF biocomposites loaded into PP.

desiccator before placing on the specimen holder. The loading quantification of lysozymes in nanoparticles was carried out with a bicinchoninic acid (BCA)[49] protein assay kit according to the manufacturer's instructions. Standard curves were prepared using BSA (Sigma-Aldrich) in concentrations ranging from 0.2 to 1 mg/mL. Lysozyme encapsulation efficiency was calculated according to eq 1.[50,51] Details of nanoparticle characterization are presented in the Supporting Information (SI).

$$\%\text{encapsulation efficiency (\%EE)} = \frac{\text{amount of protein in NPs}}{\text{initial amount of protein in water}} \times 100 \quad (1)$$

2.4. In Vitro Protein Release. Phosphate-buffered saline (PBS) solution was used to disperse lysozyme-loaded PEG−PLGA nanoparticles inside a dialysis tube at 37 °C under magnetic stirring. At predefined intervals, samples were obtained from the outer chamber of the dialysis tube and replaced with a new medium kept at the same temperature. Collected samples were then quantified with the BCA assay procedure, and the percent release and cumulative percent release of lysozyme were measured according to eqs 2 and 3[47,52]

$$\%\text{release} = \frac{\text{amount of lysozyme released at time } t}{\text{total amount of lysozyme within the NPs}} \times 100 \quad (2)$$

$$\%\text{cumulative release} = \frac{\text{volume withdrawn}}{\text{volume of chamber}} \times \%\text{release at time } t + \sum \%\text{release at time } t-1 \quad (3)$$

In order to validate that the released lysozymes were stable in nature, an enzyme-linked immunosorbent assay (ELISA) was conducted, where an antibody specific for lysozyme was precoated onto a microplate. Timely released lysozyme samples and standards were pipetted into the wells with a biotin-conjugated lysozyme; thus, a competitive inhibition reaction was launched between the lysozyme and the biotin-conjugated lysozyme with the precoated lysozyme antibody. Finally, after the substrate solution was added, color development occurred in the wells, which is opposite to the amount of lysozyme bound in the initial step, and the absorbance was measured at 450 nm.[53] Details of the ELISA methods are provided in the Supporting Information (SI).

2.5. Protein Structural Characterization. To investigate the lysozyme conformational changes and stability after its encapsulation inside PEG−PLGA nanoparticles (PP-L) or lysozyme@ZIF-encapsulated PEG−PLGA systems (PP-ZL), circular dichroism (CD) measurements were carried out at room temperature. In all formulations (L, PP-L, and PP-ZL), the lysozyme concentration was kept constant (100 μg/mL), as measured by the BCA assay before the CD spectroscopy. To investigate the molecular conformation of different formulations (L, PP-L, Z, PP-ZL), Fourier transform infrared (FTIR) spectroscopy was employed in the attenuated total reflection (ATR) mode. To probe the local backbone dynamics of the encapsulated lysozyme, electron paramagnetic resonance (EPR) spectroscopy was employed in the continuous wave (CW) mode.[54] Details of these measurements are presented in the Supporting Information (SI).

2.6. Protein Activity Assay. Lysozyme bioactivity was analyzed by a turbidimetric assay using *M. lysodeikticus* cells as the substrate.[55,56] The lysis rate of the cells by lysozymes was determined by UV spectroscopy.[57] The principle is to monitor the optical density (OD) at 450 nm of the *M. lysodeikticus* cells as the lysozyme is added.[46] A decrease in OD450 is related to the amount of substrate being degraded by the lysozyme and can be used to assess lysozyme activity.[58] Details of these measurements are presented in the Supporting Information (SI).

2.7. Cytotoxicity and Cellular Uptake Analysis of Nanoparticles. In vitro, the cytotoxicity of PEG−PLGA nanoparticles for both lysozyme loaded and unloaded systems was evaluated using a resazurin-based assay, also known as the Alamar Blue assay.[51,52,59] Confocal microscopy was utilized to investigate the cellular uptake of lysozyme-encapsulated ZIF-bound PEG−PLGA nanoparticles, and ImageJ software was used to quantify the calculated corrected total cell fluorescence (CTCF) from the confocal microscopy images. Details of the involved measurements are presented in the Supporting Information (SI).

3. RESULTS AND DISCUSSION

3.1. Preparation and Characterization of Lysozyme-Encapsulated Nanoparticles. The nanoprecipitation technique was used to prepare both lysozyme-loaded (PP-L) and lysozyme@ZIF-encapsulated PEG−PLGA nanoparticles (PP-ZL). Due to substantial stability and high coverage density, nanoprecipitation of the amphiphilic copolymer is considered to be a favorable approach for developing PEGylated nanoparticles using PEG−PLGA-type block copolymers.[60] Nucleation, growth, and aggregation are the three stages of nanoparticle production. The mixing process, which causes homogeneous supersaturation and polymer nucleation, is crucial to the outcome of nanoprecipitation. Therefore, we added the polymer-dissolved organic solvent in the water in the absence or presence of lysosomes or lysozyme@ZIF under magnetic stirring conditions. As reported earlier, an inadequate nucleation rate and larger particle growth are the results of poor mixing. As the polymer aggregation happens in the presence of larger portions of the organic solvent, we attempted to maintain the mixing speed faster than the aggregation time scale. In this way, formation of more nuclei and the aggregation of particles were favored.[61,62]

The hydrodynamic diameters (R_h) of all different formulations of nanoparticles were then determined via DLS (Figure 2A), where the diameter of each formulation was computed from the diffusion coefficient of the measured sample. The measured low polydispersity index (PDI: 0.1 to 0.3) indicates uniform particle size. The organic solvent (DMSO) used in the process of nanoparticle formation was discarded through an overnight dialysis process with a dialysis membrane in which DMSO can freely diffuse out of the nanoparticle solution. As such, the organic solvent might not be the reason for size differences. We used the dynamic light scattering method to determine the hydrodynamic size of the particles. Particle hydrodynamic diameter is correlated with Brownian motion. The DLS device will produce a correlation function that is mathematically related to particle size and its time-dependent light scattering capacity; a smaller particle will disperse more quickly than a larger one.[63] We used control experiments under similar conditions, where no ZIF was used. We did not observe any increment of the size under such circumstances. As such, our approximation is that ZIF is

https://doi.org/10.1021/acsami.3c16534
ACS Appl. Mater. Interfaces 2024, 16, 14405−14420

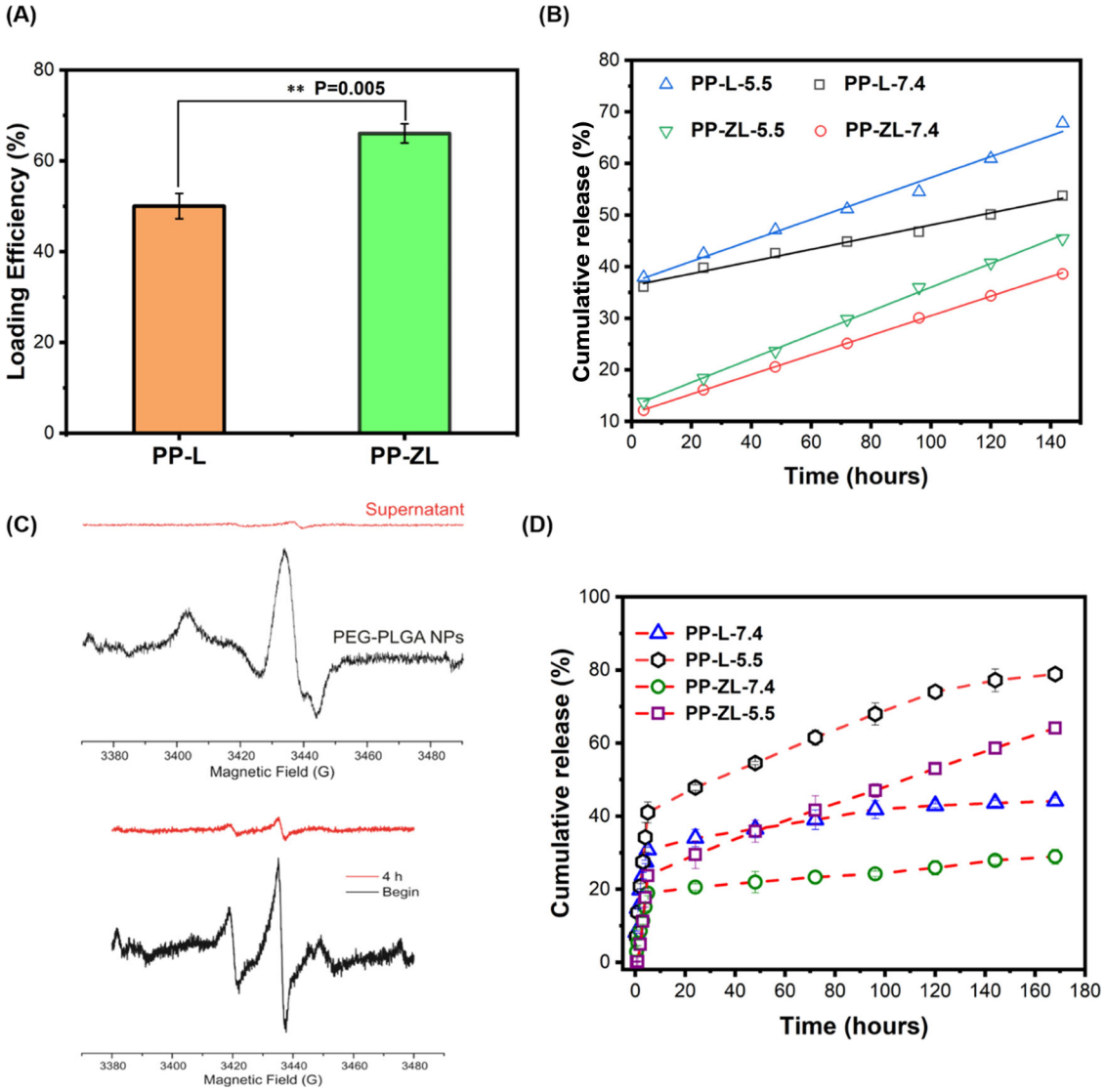

Figure 3. (A) Lysozyme loading inside PEG−PLGA nanoparticles. The loading efficiency of the lysozyme is higher in PP-ZL than in the PP-L system. (B) Release study of the lysozyme from PEG−PLGA nanoparticles in PBS media at pH 7.4 and pH 5.5. Cumulative release shows pH 5.5 released more lysozyme than pH 7.4 media in both PP-L and PP-ZL systems. (C) Top: EPR signals in the supernatant (red) and nanoparticles (black) after loading under the same loading conditions. Bottom: Release of spin-labeled protein as indicated by the decrease in EPR signal at the beginning (black) and 4 h after the release test (red). (D) ELISA assay shows the released lysozymes are identified as stable and the PP-L system releases more lysozymes than the PP-ZL system in both pH 7.4 and pH 5.5. Error bars represent the standard deviation of the average of three measurements ($N = 3$). Statistical analysis based on two-sample assuming unequal variances two-tail t test, ns for $P > 0.05$, * for $P \leq 0.05$, ** for $P \leq 0.01$, and *** for $P \leq 0.001$.

immobilized or accommodated within the hydrophobic domain of the nanoparticles, causing an expansion of the nanoscale confinement that led to the expansion of the sizes of these nanoparticles. Based on this mechanism and from our results shown in Figure 2A, the hydrodynamic diameter of the lysozyme alone was 2.26 ± 0.96 nm, in accordance with earlier reports.[64,65] The diameter of PEG−PLGA nanoparticles (PP) was found to be 163 ± 17 nm, close to the 178 ± 19 nm diameter reported by Li et al. and other authors;[66] the size difference could be due to the different organic solvent and the MW of the PEG used. The size of the lysozyme-encapsulated PEG−PLGA nanoparticles (PP-L; 219 ± 23 nm) was found to be slightly higher than that of the PEG−PLGA nanoparticles (PP) alone. Such an increase is likely caused by lysozymes encapsulated within the nanoparticles.[67] A similar increase in size was noticed too when drugs were encapsulated in PEG−PLGA-based nanoparticles when compared with drug-free nanoparticles.[50] The R_h of ZIF particles was found to be 450 ± 40 nm, close to the literature-reported value found by Yahia et al. and others.[68] The encapsulation of ZIF increased the overall size of the polymeric particles. When the lysozyme@ZIF composite was encapsulated by a PEG−PLGA system (PP-ZL) through self-assembly, the hydrodynamic diameter increased to 794 ± 47 nm. These particle size data suggested that lysozymes or lysozyme@ZIF were packed inside the PEG−PLGA nanoparticles during the nanoprecipitation process, which in turn increased the nanoparticle size.

The electrostatic repulsion or attraction between particles is governed by the electrostatic charge on the particle surface, which can be evaluated by measuring the zeta (ζ-) potential measurement. Usually, particles with elevated ζ-potential can provide kinetic and electrostatic stabilization to colloidal

https://doi.org/10.1021/acsami.3c16534
ACS Appl. Mater. Interfaces 2024, 16, 14405−14420

particles acting against particle aggregation.[69] Strong electrostatic repulsive forces between the nanoparticles are ensured by ζ-potential > +15 mV or < −15 mV, which are typically regarded as optimum for achieving good colloidal stability.[51,70] In our case, protein-free nanoparticles showed a ζ-potential of −38.8 ± 0.86 mV. Most of the earlier reports assured similar potential values for PEG−PLGA-type nanoparticles.[70] This negative potential originates from the presence of an ether bond, hydroxyl groups, and negatively charged alkoxide ions within the PEG domain.[70] Encapsulating the cationic lysozyme (under neutral pH due to the high isoelectric point of the lysozyme, pI ∼ 11.2) neutralizes the negative charge of PEG−PLGA nanoparticles (PP) to some extent. Therefore, lysozyme-encapsulated PEG−PLGA nanoparticles (PP-L) showed a suppression of the ζ-potential to −20.8 ± 0.99 mV (Figure 2B). However, both ZIF systems (Z and PP-ZL) showed a positive ζ-potential, most likely due to the presence of excess zinc ions on the particle surface.[32] The strongly positive ζ-potential of ZIF (25.93 ± 0.54 mV) became slightly reduced in PP-ZL (16.03 ± 0.81 mV), possibly via an interaction with PEG−PLGA nanoparticles. This experiment suggested that both the PP-L and PP-ZL systems demonstrate both kinetic and electrostatic stability, favoring their persistence in a colloidal state.

The morphology observed in the TEM images (Figure 2C−E) validated the observation revealed by DLS and ζ-potential measurements. The PEG−PLGA nanoparticles were spherical, with a smaller mean diameter than lysozyme-encapsulated PEG−PLGA nanoparticles, supporting the DLS analysis and in accordance with the literature.[50,71] The TEM image of ZIFs (Figure 2E) showed a hexagonal morphology inside a PEG−PLGA nanoparticle. This hexagonal shape is formed by distorting the water-driven hydrogen-bonding interactions between the monodentate methylimidazole in one direction and the free imidazole in another direction.[72] When the lysozyme@ZIF composite was encapsulated within the PEG−PLGA nanoparticles (PP-ZL), its morphology became spherical, indicating that the PEG−PLGA layer surrounded the hexagonal lysozyme@ZIF composite. Although the results of TEM and DLS analyses were not precisely the same because of the technical difference (the hydrodynamic diameter in the suspension is measured using DLS, while the gyration radius of dry particles is measured using TEM images[61]), both the TEM and DLS analyses were coherent in trend.

3.2. Protein Encapsulation and Release. In the nanoprecipitation process of PEG−PLGA, the PEG chains are exposed on the surface of a nanoparticle as the PLGA block collapses into the core. This is because of the hydrophobic interactions that drive the self-assembly of PEG−PLGA.[73] Lysozyme has a net positive charge because of its high pI and, hence, presents a hydrophilic surface.[74] Therefore, the encapsulation of lysozymes during nanoprecipitation could unfold the protein slightly to wrap itself within the hydrophobic PLGA core of the PEG−PLGA nanoparticles. Alternately, the protein could also maintain its secondary structure and wrap around the PEG shell. Both could occur, too, with different chances. Note that the immobilization of the lysozyme in the PEG shell may not be stable and likely lead to protein loss due to leaching. Bearing this in mind, we noticed a decent amount of lysozyme encapsulation in the PEG−PLGA-bound lysozyme@ZIF system (PP-ZL; 66.04 ± 2.11%) compared to those demonstrated by PEG−PLGA-lysozyme (PP-L; 50.05 ± 2.79%) particles (Figure 3A). This differentiation was also statistically significant ($P < 0.05$) based on the two-sample two-tail t test shown in Figure 3A. The most likely reason for the low encapsulation efficiency of PP-L might be that the lysozyme is relatively hydrophilic with polar group activities, which does not favor the contact with the hydrophobic PLGA core (while the PEG shell only offers weak interactions);[45] unfolding the protein to expose hydrophobic residues and letting them collapse with the PLGA segment is obviously not favored. On the contrary, the encapsulation of the lysozyme in the ZIF system does not face this problem because it was pre-encapsulated before nanoprecipitation with PEG−PLGA. Moreover, the two-layer system involving ZIF keeps the lysozyme inside of the system from leaching, as ZIF can block the diffusion of the lysozyme into the continuous (or the bulk) phase. Lastly, ZIFs are often considered hydrophobic (when Zn^{2+} was removed) and favored to be wrapped by the hydrophobic core of PLGA. Therefore, more lysozymes were encapsulated in the ZIF-associated systems (PP-ZL).

A lysozyme release study at pH 7.4 was then carried out in phosphate-buffered saline (PBS) at 37 °C. PBS was chosen because it can mimic the isotonicity of the physiological fluid.[52,75] Release studies were conducted at both pH 7.4 and pH 5.5 to imitate normal tissue conditions and inflammatory microenvironment conditions, respectively, for 140 h. The amount of released protein was first quantified by a BCA assay and analyzed with the help of eq 3.[76,77] We observed a biphasic release, the linear phase of which started after 4 h, and it is shown in Figure 3B. We found that the encapsulation of lysozymes in PEG−PLGA nanoparticles, within or without ZIF, extensively sustained the release of the protein. Even after 140 h, the protein release was not complete from these systems in either pHs. We indeed noticed a more significant reduction of the initial burst release (0−4 h) of lysozymes from nanoparticles for the PP-ZL (lysozyme@ZIF in particles) system than that of PP-L (lysozyme in particles) systems for both pH conditions (pH 7.4 and pH 5.5). While PP-ZL released 12% (pH 7.4) and 13% (pH 5.5) of the encapsulated lysozymes in the first 4 h, PP-L released 36% at pH 7.4 and 37% at pH 5.5 of the loaded protein. One of the most likely reasons for the higher burst rate of PP-L was the penetration of water into the PLGA domains and the diffusion of lysozymes into the release medium. The PEG chain permitted water uptake via hydration, which created more water channels inside the polymer matrix, placing the protein directly in contact with the bulk medium. Similar outcomes of high burst release have frequently been observed in the literature for block copolymeric systems.[78,79] On the contrary, PP-ZL's two layers protected lysozymes from leaching because the water penetration rate was lower due to the internal ZIF scaffolds within PEG−PLGA nanoparticles. Another likely reason was the release of lysozymes adjacent to the PEG−PLGA nanoparticle surface, which was caused by the efflux of organic solvents during the nanoprecipitation step, pulling some lysozymes away from the nanoparticles core.[79,80] After the initial burst release, lysozymes were released slowly because the protein was taken away from the deeper parts of the nanoparticles, and after 7 days, PP-L showed 53 and 64% lysozyme release at pH 7.4 and 5.5, respectively, whereas PP-ZL showed 38 and 45% release at pH 7.4 and 5.5, respectively. In both nanoparticle platforms, decreasing the pH of the release media increased the overall lysozyme release. This is because the ionic strength of the release media increased the

https://doi.org/10.1021/acsami.3c16534
ACS Appl. Mater. Interfaces 2024, 16, 14405−14420

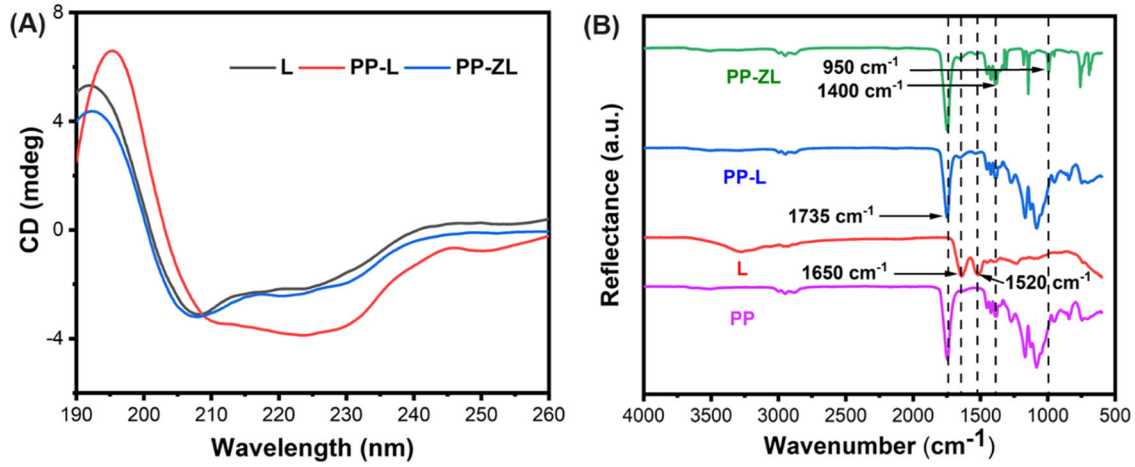

Figure 4. (A) Circular dichroism (CD) spectra of the lysozyme and lysozyme encapsulated in PP-L and PP-ZL. (B) FTIR spectra with the lysozyme, PEG−PLGA nanoparticles, lysozyme encapsulated in PP, and lysozyme@ZIF encapsulated in PP in red, purple, cyan, and green, respectively.

release rate by regulating the swelling behavior of the polymer matrix, which in turn promoted lysozyme diffusion from the nanoparticles.[81] Also, ZIFs would be (at least partially) disassembled under pH 5.5 rather than pH 7.4. Therefore, we observed more lysozymes released at pH 5.5 than at pH 7.4 in both the PP-L and PP-ZL systems. We further validated the release of lysozymes from nanoparticles via EPR using spin-labeled lysozymes (Figure 3C). The top panel of Figure 3C shows the EPR signals in the supernatant (red) and nanoparticles (black) after loading under the same loading conditions, indicating nanoparticles stabilize the encapsulated lysozymes. This experiment also revealed that the release of the spin-labeled protein was manifested by the decrease in the EPR signal at the beginning (black) and 4 h after the release test (red) (Figure 3C, bottom panel).

It is important to know if the released protein is structurally and functionally active over the extended period. Therefore, we used ELISA to examine the structural integrity of lysozymes released from PP-L or PP-ZL systems. An ELISA-based quantification method is widely used for the analysis of proteins because of its sensitivity and specificity.[82] In the ELISA assay, an antibody specific for an enzyme is precoated onto a microplate. Then, the antigen is allowed to react with the specific antibody, which is detected by an enzyme-labeled secondary antibody. When an antigen is present, a chromogenic substrate is used to create color, which ultimately quantifies the antigen's quantity (lysozyme).[83] The complete biphasic release profile, where the lysozyme has been quantified by the ELISA assay, is shown in Figure 3D, which is coherent with our BCA assay-based release detection shown earlier in Figure 3B. The main focus of this ELISA assay was to check the stability of the release lysozyme, and our result indicated that the lysozymes remained stable after 7 days of release.

3.3. Structural Characterization of Proteins. To probe the secondary structure of proteins in solution or upon encapsulation, CD spectra in the far-UV region (190−240 nm) were collected for lysozymes in this study.[84] Lysozymes are composed of mainly α-helices and β-strands.[64] The Protein Data Bank shows that the secondary structure of lysozymes contains α-helices (34−42%) and β-sheets (7−12%).[85] Therefore, lysozyme is an α-helix-rich protein. Two negative bands at 208 and 222 nm, which correspond to the $\pi \rightarrow \pi^*$ and $n \rightarrow \pi^*$ electronic transitions for the α-helix secondary structure, respectively, were visible in the distinctive CD spectra of the bare lysozyme shown in Figure 4A, black. However, in PP-L, a decrease in the magnitude of molar ellipticities (mdeg) was observed with a clear shift in peak positions as compared to lysozymes in solution (Figure 4A, red versus black). Such a difference could be caused by the interference of PEG−PLGA with the lysozyme, which may perturb the α-helix hydrogen-bonding networks[86] and partially unfold the encapsulated protein. In PP-ZL (Figure 4A cyan), when lysozyme@ZIF composites were encapsulated within PEG−PLGA nanoparticles, the characteristic peak positions of the α-helix were retained although the peak intensity was reduced. This indicates that ZIF helps prevent protein unfolding upon encapsulation in the nanoparticles.

Fourier transform infrared (FTIR) spectroscopy (Figure 4B) was then employed to examine the tertiary structure of the lysozyme encapsulated in the nanoparticles and compare it to that of the native lysozyme. A protein's tertiary structure is linked to distinctive amide-I (1600−1700 cm^{-1}) and amide-II (1500−1600 cm^{-1}) bands in the mid-IR region.[32] A change in the structure has less impact on the amide-I band, which is associated with C═O stretching, than on the amide-II band, which is primarily tied to the coupling between C−N stretching and N−H bending.[87] In our study, the amide-I and amide-II bands of pure lysozyme (L) were found at 1650 and 1520 cm^{-1} (Figure 4B), respectively, consistent with the literature.[88] These two amide bands were present in both lysozyme-encapsulated nanoparticles, i.e., PP-L and PP-ZL, demonstrating that the tertiary structures of lysozyme are quite stable. Based on the strengthened carbonyl absorption at 1735 cm^{-1} attributed to the ester bond, the FTIR data (Figure 4B) also showed the presence of a PLGA block in all PEG−PLGA systems (PP, PP-L, and PP-ZL). With the absorption of C−N bonds, IR peaks between 950 and 1400 cm^{-1} in the ZIF-involved system and the absorption band at 421 cm^{-1} demonstrate the presence of Zn−N stretching.[89] Based on CD and FTIR data, lysozyme encapsulation to nanoparticles seems to affect the protein secondary structure to different extents but not the tertiary structure. ZIFs were effective in reducing the perturbation to the lysozyme secondary structure.

https://doi.org/10.1021/acsami.3c16534
ACS Appl. Mater. Interfaces 2024, 16, 14405−14420

For long-term stability from both chemical and physiological standpoints, our proposed system showed a very decent performance. There were no signs of physical stability issues, including sedimentation and agglomeration of PEG−PLGA nanoparticles, after 1 month from preparation. After 7 days of release, our system's encapsulated lysozyme showed excellent results in BCA and ELISA assays. The intact peptide bonds of the released lysozyme reduced the copper(II) sulfate Cu^{2+} ion to Cu^{1+}, which was detected by the BCA assay, and this reduction was equivalent to the amount of lysozyme presented in the solution. Similarly, in the enzyme-linked immunosorbent ELISA assay, a lysozyme-specific antibody was able to bind with the released lysozyme and quantify the lysozyme bindings after 7 days of release. Thereby, from a chemical standpoint, this system was able to keep intact the lysozyme stability.

3.4. Protein Dynamics and Location. To probe the local backbone dynamics and the possible local environment of lysozymes in various nanoparticles, we carried out site-directed spin labeling (SDSL) in combination with electron paramagnetic resonance (EPR) studies. Detailed procedures have been published in various studies.[90−92] In brief, we selectively attached an EPR spin label to three representative sites of the lysozyme, namely, residues 44, 65, and 151, one at a time, following the scheme shown in Figure 5 inset. In solution, the

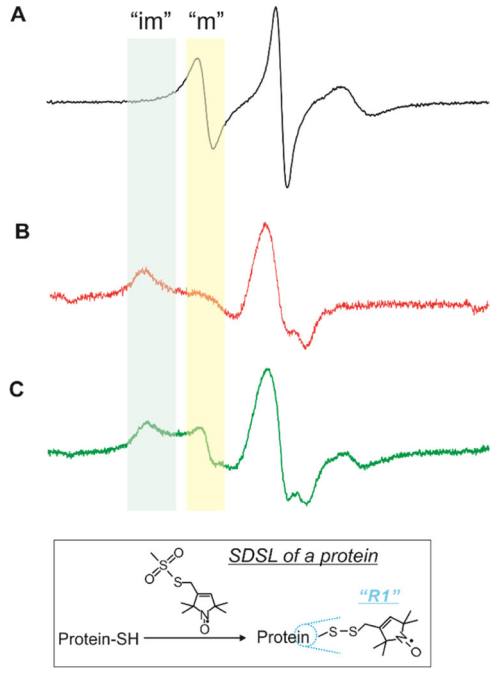

Figure 5. EPR data on proteins in solution (A), PEG−PLGA nanoparticles (B), and ZIF/PEG−PLGA nanoparticles (C). (Inset) Schematic illustration of the SDSL of a protein residue.

CW EPR spectrum of each labeled protein mutant shows a relatively narrow spectral line width (Figure 5A), which is known to be caused by the averaging of rapid protein rotational tumbling, backbone fluctuation, and spin-label side-chain motion.[93−95] Upon encapsulation in PEG−PLGA, the EPR spectrum became extremely broadened (a representative spectrum is shown in Figure 5B), suggesting that all three kinds of motions were restricted, likely due to the complete immobilization of the lysozyme in the nanoparticle. Spectral simulations detailed in the SI showed a two-component spectrum with a dominant (~75%; Table S1) component consistent with the well-known, immobile component in EPR simulations,[96] which is characterized by a highly restricted slow motion (see the low R_z and the high c_{20} and c_{22} parameters for the "im" component in Table S1) and a nonpolar environment (see the low A_{zz} parameter for the "im" component in Table S1). The less dominant component (~25%), on the other hand, is the "mobile" component commonly seen in EPR simulation, which displayed enhanced motion with less restriction in space (see the high R_z and the low c_{20} and c_{22} parameters for the "m" component in Table S1) and a nonpolar environment (see the high A_{zz} parameter for the "m" component in Table S1). Thus, the encapsulated protein is mostly located in a crowded, nonpolar environment (likely the PLGA core) although partial distribution to the less-crowded, polar shell is possible. When the same measurement was carried out for the spin-labeled protein protected by ZIFs upon encapsulation in PEG−PLGA, the resultant CW EPR spectrum also showed two components (Figure 5C), with one consistent with immobilized motion (the immobile component) as the dominant case of Figure 5B and the mobile component with a relatively high mobility (the mobile component). In this case, the mobile component is the dominant one now. Spectral simulation confirms this observation, wherein the relative contributions from the mobile and immobile components become ~59 and ~41% although the rate, polarity, and motion parameters did not change drastically (Table S1). This means ZIF offers nearly 35% more (59 vs 25%) mobile component to the encapsulated protein to the hydrophilic shell without major leaching. This finding is consistent with our previous study on protein immobilization in ZIF, which did offer some degree of freedom as some protein molecules can be partially exposed above the ZIF surface.[96] The immobile component likely originated from the labeled protein site in contact with the ZIF scaffold, while the mobile one from the protein is exposed partially above the ZIF surface. Thus, EPR studies suggested possible protein locations in the PP core and inside of ZIFs in PP-ZL.

3.5. Bioactivity Study of Proteins. Lysozymes can break down the β-(1,4)-glycosidic bonds between *N*-acetylmuramic acid (NAM) and N-acetylglucosamine (NAG) of peptidoglycan chains. Gram-positive bacteria (*M. lysodeikticus*) have cell walls made of multiple peptidoglycan layers, which lack an outer membrane and are joined to the peptidoglycan by polysaccharides, lipoteichoic acids, and teichoic acids.[97,98] Therefore, lysozyme activity can cause bacterial cell lysis and eventually death of the bacterial cell.[99] The principle to monitor the activity of the lysozyme is to observe the optical density (OD) at 450 nm of *M. lysodeikticus* cells after adding the lysozyme. The degradation of *M. lysodeikticus* cells by the lysozyme is indicated by the decrement of OD_{450}. The concentrations of all lysozyme formulations (L, PP-L, and PP-ZL) were kept the same (100 μg/mL). Our activity study (Figure 6) showed all of the lysozyme-encapsulated systems were bioactive. From the results (Figure 6A), the blank (only the media) and the negative control, i.e., PEG−PLGA nanoparticles (PP), did not show any drop in OD at 450 nm, as both of them did not contain a lysozyme. Similar results were noticed in the literature for the control study.[46] The BCA assay was utilized to measure the lysozyme concentrations at all tested formulations. The positive control, which is the bare lysozyme (L), exhibited the highest unit of activity (156.6 ± 7.33), as depicted in Figure 6B in the main manuscript. In comparison, lysozymes encapsulated within PEG−PLGA

https://doi.org/10.1021/acsami.3c16534
ACS Appl. Mater. Interfaces 2024, 16, 14405−14420

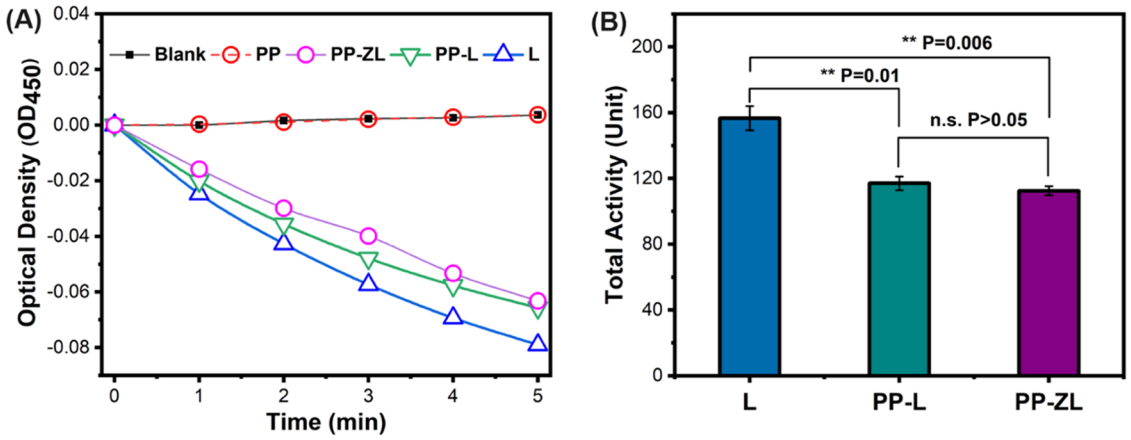

Figure 6. Antibacterial activity of the lysozyme-encapsulated systems. (A) Reduction of optical density at 450 nm indicates the function of lysozymes on the cell lysis of *M. lysodeikticus* bacterial cell walls. (B) Total activity calculated from the optical density shows lysozymes that encapsulate inside the PEG−PLGA nanoparticles and lysozymes that encapsulate in the PEG−PLGA-bound ZIF system both have almost similar cell lysis rates. Error bars represent the standard deviation of the average of three measurements ($N = 3$). Statistical analysis based on two-sample assuming unequal variances two-tail t test, ns for $P > 0.05$, * for $P \leq 0.05$, ** for $P \leq 0.01$, and *** for $P \leq 0.001$.****

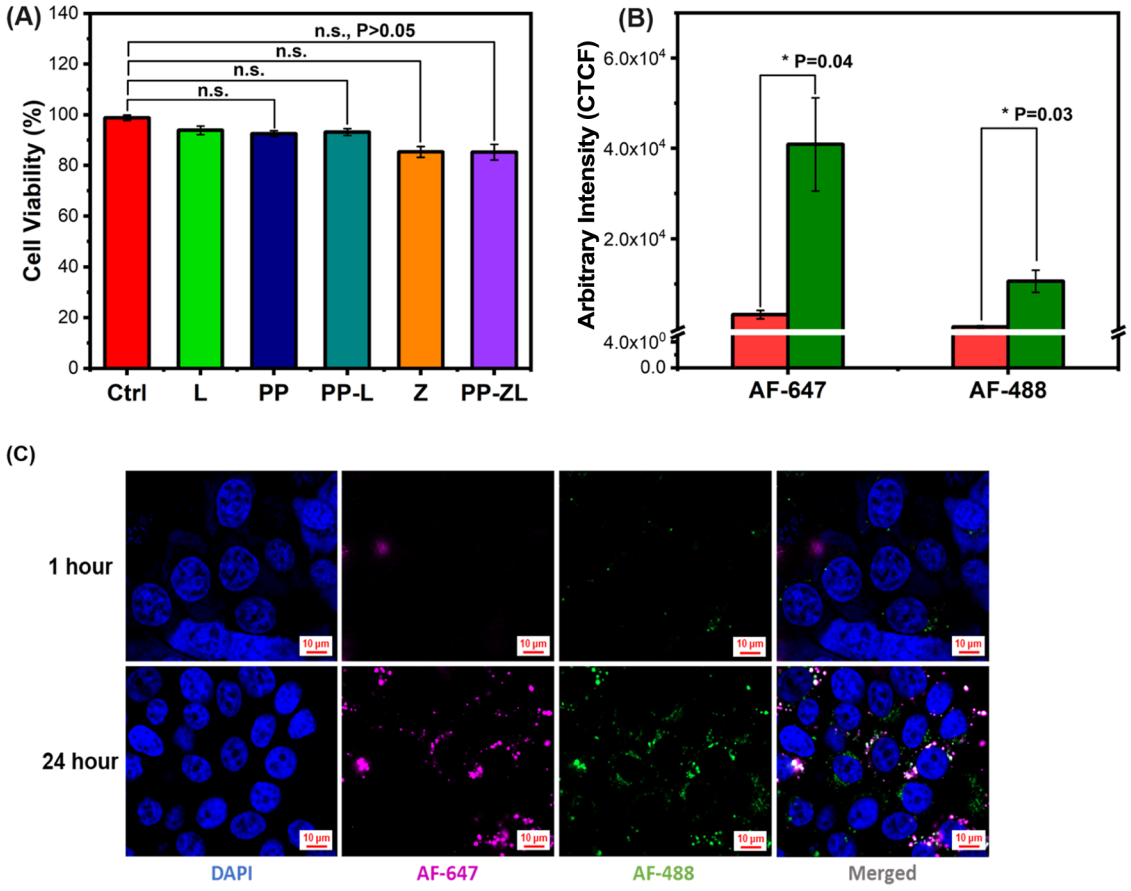

Figure 7. (A) Cytotoxicity study of lysozyme-encapsulated systems on the mouse fibroblast cell (L929). None of the compounds showed any toxic effects; therefore, the cell viability was more than 85% after 48 h of seeding and 24 h of incubation in the presence or absence of nanoparticles. (B) Cellular uptake studies of fluorescence intensity accounted by calculating the corrected total cell fluorescence (CTCF) from BxPC3 cells; error bars represent the standard deviation of the average of three measurements ($N = 3$). (C) Cellular uptake study of lysozyme-loaded PEG−PLGA nanoparticles for 24 h. Posttreatment cells were fixed with 4% PFA at 1 and 24 h and imaged under a confocal microscope using DAPI, AF-647, and AF-488 filters. Blue color indicates the cell nucleus, purple color indicates PEG−PLGA-AF-647 nanoparticles, and green color indicates lysozyme-AF-488. The merged image demonstrates the accumulation of nanoparticles in the cytoplasmic area of the cell. (Error bars represent the standard deviation of the average of three measurements ($N = 3$); statistical analysis based on two-sample assuming unequal variances two-tail t test, ns for $P > 0.05$, * for $P \leq 0.05$, ** for $P \leq 0.01$, and *** for $P \leq 0.001$).

nanoparticles (PP-L) displayed a lower unit of activity (117 ± 4.16), and the PEG−PLGA-bound lysozyme@ZIF system (PP-ZL) demonstrated a slightly decreased unit of activity (112 ± 2.76) than PP-L systems. The two-tailed t test did not

https://doi.org/10.1021/acsami.3c16534
ACS Appl. Mater. Interfaces 2024, 16, 14405−14420

reveal any statistically significant ($P > 0.05$) difference between the bioactivity of the PP-L and PP-ZL systems. However, the observed variations between the free lysozyme (L) and the lysozyme encapsulated in nanoparticles (PP-L and PP-ZL) were likely due to the nanoparticles obstructing enzyme access to the bacterial cell wall. Additionally, the extra layer in PP-ZL hindered enzyme attack on the substrate, further reducing the activity. Although the enzymatic degradation rate was diminished, both forms of enzyme encapsulation exhibited the inherent activity of the enzyme.[46] Between PP-L and PP-ZL systems, PP-L demonstrated enhanced activity compared to PP-ZL, likely due to the faster leaching rate of the PP-L-bound enzyme compared to its PP-ZL counterpart. Nevertheless, our results indicated that both systems (PP-L and PP-ZL), regardless of ZIF-mediated encapsulation, remained functionally active despite the slight loss of intrinsic activity compared to the free lysozyme. Moreover, the reduced activity can be compensated by the prolonged release and augmented protection of lysozymes observed in our release study, ensuring an extended enzymatic effect. We can say there is no significant difference between the PP-L and PP-ZL systems (statistical analysis also proved that). We are approaching the problem toward extending the stability of encapsulated lysozymes. We showed that the PP-ZL system showed prolonged release of stable (ELISA) enzymes compared to the PP-L system; therefore, the PP-ZL system is more promising for certain biological applications for which retention of enzymatic actions for a longer period is desired.

3.6. Cytotoxicity Study of Protein-Encapsulated Nanoparticles. In biomedical applications, the biosafety of protein carrier nanoparticles must be assessed. PEG−PLGA nanoparticles are well-known for their biocompatibility and biodegradability for both in vivo and in vitro studies.[100,101] However, the threshold concentration of ZIF determines its biocompatibility. As ZIF is produced by 2-methylimidazole and zinc ions, where zinc ions may enhance reactive oxygen species (ROS production), DNA damage may occur above the threshold concentration. Literature shows zinc concentrations less than 30 μg/mL can be biocompatible.[102] An in vitro cytotoxicity study (Alamar blue assay) was conducted to assess the cell viability of the various formulations of PEG−PLGA nanoparticles with encapsulated and nonencapsulated lysozymes upon their exposure to the mouse fibroblast cell line (L929) with $N = 3$ replication. Alamar blue assay showed (Figure 7A) excellent cell viability (more than 80% of the cells were alive) for all of the formulations with 20 μg/mL concentration of nanoparticles. All of the four controls, i.e., cells without nanoparticles (Ctrl), lysozyme (L) only with cells, PEG−PLGA nanoparticles (PP) with cells, and ZIF (Z) nanoparticles with cells, showed a sufficient amount of cell viability. The lowest cell viability among the controls was ZIF nanoparticles (Z), which was still ∼85%, indicating a decent biocompatibility of the ZIF system at this concentration. The other formulations such as lysozyme-encapsulated PEG−PLGA nanoparticles (PP-L) provided more than ∼90% cell viability and the PEG−PLGA-bound lysozyme@ZIF system (PP-ZL) provided ∼86% cell viability after the restriction of ZIF discussed above. It should be noted that the proliferation of cells was observed after 48 h of seeding. The variation of this viability was observed because of different formulations of nanoparticles along with their preparation materials. However, the t test showed there is no statistical significance ($P > 0.05$) between the control (ctrl) and different nanoparticles' formulations in terms of cell viability. Therefore, overall results indicated that the cytocompatibility of the studied samples was reasonable. Future studies will take into account more precise cell proliferation assays, such as assays based on DNA quantification, to confirm this effect as DNA replication that must take place before cell division.

3.7. Cellular Uptake of Nanoparticles. The cellular uptake of lysozyme-loaded PEG−PLGA nanoparticles was evaluated by confocal microscopy analysis. The nanoparticles were internalized into cells through endocytosis, where the cell membrane engulfs the nanoparticles into a vesicle.[103] Endosomes, lysosomes, and other vesicular structures are most likely involved in the transport of the encapsulated nanoparticles through the endolysosomal membrane system. It is important for lysozyme-encapsulated nanoparticles to escape from the lysosome or endosome to reach the targeted destination within the cell where lysozyme release can occur. The nanoparticles can achieve endosomal escape either by endosomal rupture (mediated by disturbed osmotic pressure within the endosome triggered by nanoparticles) or by membrane fusion. By using techniques like the proton sponge effect, where an input of protons causes osmotic swelling and endosome rupture, nanoparticles can be promoted to endosomal escape.[104] An endosome acidic environment causes PLGA to hydrolyze and break down, releasing acidic byproducts in the process.[81] The pH within the endosomes is decreased by this mechanism. Because PLGA nanoparticles can absorb protons, they are known to function as proton sponges. To preserve electrochemical balance, PLGA nanoparticles absorb protons as the pH drops inside the endosomes, which results in an inflow of chloride ions. The endosomes absorb water as a result of the osmotic imbalance brought about by the ion inflow, which causes them to enlarge and finally rupture.[105] Thus, PEG−PLGA nanoparticles and their cargo are released into the cell's cytoplasm as a result of this breakdown of endosomal membranes. In the cytoplasm, both PEG−PLGA and ZIF can be dissociated and therefore release the lysozyme.

In our proposed system, we labeled the enzyme with Alexa Fluor 488 and the nanoparticle with Alexa Fluor 647 fluorescent dye. The cellular uptake of protein delivery is robust and is comparable to various nanoparticle systems constructed by others. We also observed a time dependence on the extent of uptake. As shown in Figure 7B−C, a significant difference in fluorescence intensities was observed between different time intervals. At the end of 24 h, nearly 5-fold higher cellular internalization was observed compared to the initial hour for lysozyme-encapsulated PEG−PLGA nanoparticles, which indicates the proposed system's decent cellular uptake compatibility. In the literature, we have noticed a similar time-dependent increase in the amount of dye-loaded nanoparticles for cellular uptake. Long et al. reported a 2-fold increment of their rhodamine B-loaded PLGA nanoparticles' cellular uptake in 3 h of study.[106] Devrim et al. reported more than 80% cellular uptake of dye-labeled lysozyme-loaded lipid-polymer hybrid nanoparticles. This is because the lipid monolayer coating of nanoparticles increased the cell membrane interaction with time.[107] Zhao et al. reported courmarin-6-loaded Di-PEG-ZIF nanoparticles showed 1.8-fold cellular uptake in Lncap cells in 2 h of study.[108] For our proposed system, it could be possible that nanocarriers were internalized through the endocytosis process, in which the nanoparticles initially stayed in the cytoplasm before lysozyme is released and traveled to the nuclear or perinuclear region.[109] However,

https://doi.org/10.1021/acsami.3c16534
ACS Appl. Mater. Interfaces 2024, 16, 14405−14420

we also observed colocalization of intracellular fluorescence after 24 h, which could indicate undissociated protein and polymer particles. As such, the relative fraction between the released and particle-bound protein should be linked to the in vitro release behavior studied earlier for our systems.[66] In order to quantify the cellular uptake of lysozyme-loaded nanoparticles, the calculated corrected total cell fluorescence (CTCF) was determined (Figure 7B) by the increased cell fluorescence due to the uptake of fluorescent nanoparticles. The results showed a significant increase in CTCF for both Alexa fluor 647 tagged nanoparticles and Alexa fluor 488 tagged lysozymes after 24 h of incubation. Moreover, the results are supported by a statistical *t* test where the p-value is less than 0.05 for both AF-647 and AF-488 as compared to their 1 and 24 h incubation, indicating the differences are statistically significant. Thereby, the time-dependent uptake of fluorescently labeled nanoparticles in this experiment will help determine the prognostic and therapeutic potential of the protein delivery system.

4. CONCLUSIONS

In this study, we developed a novel approach to encapsulate a globular protein in popular PEG−PLGA nanoparticles with the assistance of ZIFs via nanoprecipitation. ZIF was the optimal candidate in this work due to its unique capability of forming protein@ZIF biocomposites via cocrystallization in the aqueous phase and therefore generalizable to proteins. Also, ZIFs can be disassembled under weakly acidic pHs, accelerating the pH-sensitive release of the protein. As compared to the direct encapsulation of a model protein into the block copolymeric nanoparticles, an additional layer of protection via ZIF prior to nanoprecipitation offered enhanced loading capacity, reduced leaching, especially in the initial stage, led to slower release kinetics, and reduced secondary structural perturbation, as determined by a standard loading and release study as well as various spectroscopic techniques. Meanwhile, the bioactivity, cytotoxicity, and cellular uptake seem to be comparable to the direct encapsulation of proteins via nanoprecipitation. Our results demonstrated the concept of using ZIF as a second layer of wrapping to assist in protein encapsulation in PEG−PLGA nanoparticles. This work is the basis of future novel polymeric nanoparticle-based protein confinement platforms, using MOFs as the second layer of encapsulation. More efforts are needed to optimize protein encapsulation and release, as well as reduce the size of protein-loaded nanoparticles, which will make this platform further suitable for therapeutic protein delivery. On this note, future work will also be needed to prove the feasibility of the developed platform in animal models. Nevertheless, this work is the first step into exploring polymeric nanoparticles as future protein confinement platforms for fundamental protein study and delivery applications.

■ ASSOCIATED CONTENT

Supporting Information

The Supporting Information is available free of charge at https://pubs.acs.org/doi/10.1021/acsami.3c16534.

Detailed description of methods and materials and EPR simulation and data (PDF)

■ AUTHOR INFORMATION

Corresponding Author

Mohiuddin Quadir − *Biomedical Engineering Program, North Dakota State University, Fargo, North Dakota 58108, United States; Department of Coatings and Polymeric Materials, North Dakota State University, Fargo, North Dakota 58108, United States;* orcid.org/0000-0003-2811-773X; Email: mohiuddin.quadir@ndsu.edu

Authors

Md Rakib Hasan Khan − *Biomedical Engineering Program, North Dakota State University, Fargo, North Dakota 58108, United States*

Zoe Armstrong − *Department of Chemistry and Biochemistry, North Dakota State University, Fargo, North Dakota 58108, United States*

Mary Lenertz − *Department of Chemistry and Biochemistry, North Dakota State University, Fargo, North Dakota 58108, United States*

Briana Saenz − *Department of Chemistry and Biochemistry, St. Mary's University, San Antonio, Texas 78228, United States*

Narendra Kale − *Department of Pharmaceutical Sciences, North Dakota State University, Fargo, North Dakota 58108, United States*

Qiaobin Li − *Department of Chemistry and Biochemistry, North Dakota State University, Fargo, North Dakota 58108, United States;* orcid.org/0000-0002-0206-1515

Austin MacRae − *Department of Chemistry and Biochemistry, North Dakota State University, Fargo, North Dakota 58108, United States;* orcid.org/0000-0002-7534-1753

Zhongyu Yang − *Department of Chemistry and Biochemistry, North Dakota State University, Fargo, North Dakota 58108, United States;* orcid.org/0000-0002-3018-3608

Complete contact information is available at: https://pubs.acs.org/10.1021/acsami.3c16534

Author Contributions

#M.R.H.K. and Z.A. contributed equally to this work. The manuscript was written through the contributions of all authors. All authors have given approval to the final version of the manuscript.

Funding

This work was supported by the National Science Foundation (NSF), grant no. CBET 2239629, to M.Q. Partial support was received by M.Q. from the National Science Foundation under NSF EPSCoR Track-1 Cooperative Agreement OIA #1946202. This work was also supported by NSF (MCB 1942596, CBET 2217474, and DMR 2306137 to Z.Y.). The authors are grateful to Dr. Peter Fajer for his generous donation of the Bruker EMX system to Z.Y. Any opinions, findings, conclusions, or recommendations expressed are those of the authors and do not necessarily reflect the views of the National Science Foundation.

Notes

The authors declare no competing financial interest.

■ ACKNOWLEDGMENTS

The authors would like to thank Scott Payne and Jayma Moore of the NDSU Electron Microscopy Core for TEM imaging. The authors thank Md Fahad Hasan, Department of Plant

Sciences, NDSU for the preparation of the supplementary cover art for this manuscript.

■ ABBREVIATIONS

PEG−PLGA, poly(ethylene glycol)-*block*-poly(lactic-*co*-glycolic acid); MOF, metal−organic framework; ZIF, zeolitic imidazolate framework; TEM, transmission electron microscopy; DLS, dynamic light scattering; EPR, electron paramagnetic resonance; SDSL, site-directed spin labeling

■ REFERENCES

(1) Chiesa, G.; Kiriakov, S.; Khalil, A. S. Protein assembly systems in natural and synthetic biology. *BMC Biol.* **2020**, *18* (1), No. 35, DOI: 10.1186/s12915-020-0751-4.
(2) Kalathiya, U.; Padariya, M.; Faktor, J.; Coyaud, E.; Alfaro, J. A.; Fahraeus, R.; Hupp, T. R.; Goodlett, D. R. Interfaces with Structure Dynamics of the Workhorses from Cells Revealed through Cross-Linking Mass Spectrometry (CLMS). *Biomolecules* **2021**, *11*, No. 382, DOI: 10.3390/biom11030382.
(3) Seisdedos, H. G.; Levin, T.; Shapira, G.; Freud, S.; Levy, E. D. Mutant libraries reveal negative design shielding proteins from supramolecular self-assembly and relocalization in cells. *Proc. Natl. Acad. Sci. U.S.A.* **2022**, *119* (5), No. e2101117119, DOI: 10.1073/pnas.2101117119.
(4) Michailidou, F. Engineering of Therapeutic and Detoxifying Enzymes. *Angew. Chem.* **2023**, *135*, No. e202308814, DOI: 10.1002/ange.202308814.
(5) Bizeau, J.; Mertz, D. Design and applications of protein delivery systems in nanomedicine and tissue engineering. *Adv. Colloid Interface Sci.* **2021**, *287*, No. 102334.
(6) Reis, C. P.; Neufeld, R. J.; Ribeiro, A. J.; Veiga, F. Nanoencapsulation II. Biomedical applications and current status of peptide and protein nanoparticulate delivery systems. *Nanomed.: Nanotechnol., Biol. Med.* **2006**, *2* (2), 53−65.
(7) Lee, J.; Mahendra, S.; Alvarez, P. J. J. Nanomaterials in the Construction Industry: A Review of Their Applications and Environmental Health and Safety Considerations. *ACS Nano* **2010**, *4* (7), 3580−3590.
(8) Wörsdörfer, B.; Pianowski, Z.; Hilvert, D. Efficient in Vitro Encapsulation of Protein Cargo by an Engineered Protein Container. *J. Am. Chem. Soc.* **2012**, *134* (2), 909−911.
(9) Gouveia, M. G.; Wesseler, J. P.; Ramaekers, J.; Weder, C.; Scholten, P. B. V.; Bruns, N. Polymersome-based protein drug delivery − quo vadis? *Chem. Soc. Rev.* **2023**, *52* (2), 728−778 10.1039/D2CS00106C.
(10) Gao, J.; Gu, H.; Xu, B. Multifunctional Magnetic Nanoparticles: Design, Synthesis, and Biomedical Applications. *Acc. Chem. Res.* **2009**, *42* (8), 1097−1107.
(11) Yeo, Y.; Park, K. Control of encapsulation efficiency and initial burst in polymeric microparticle systems. *Arch. Pharmacal Res.* **2004**, *27* (1), 1−12.
(12) Panyam, J.; Labhasetwar, V. Biodegradable nanoparticles for drug and gene delivery to cells and tissue. *Adv. Drug Delivery* **2012**, *64*, 61−71, DOI: 10.1016/j.addr.2012.09.023.
(13) Tobío, M.; Gref, R.; Sánchez, A.; Langer, R.; Alonso, M. J. Stealth PLA-PEG Nanoparticles as Protein Carriers for Nasal Administration. *Pharm. Res.* **1998**, *15* (2), 270−275.
(14) Gaucher, G.; Marchessault, R. H.; Leroux, J.-C. Polyester-based micelles and nanoparticles for the parenteral delivery of taxanes. *J. Controlled Release* **2010**, *143* (1), 2−12.
(15) Danhier, F.; Ansorena, E.; Silva, J. M.; Coco, R.; Le Breton, A.; Préat, V. PLGA-based nanoparticles: an overview of biomedical applications. *J. Controlled Release* **2012**, *161*, 505−522, DOI: 10.1016/j.jconrel.2012.01.043.
(16) Gaharwar, A. K.; Peppas, N. A.; Khademhosseini, A. Nanocomposite hydrogels for biomedical applications. *Biotechnol. Bioeng.* **2014**, *111* (3), 441−453, DOI: 10.1002/bit.25160.
(17) Zhang, K.; Tang, X.; Zhang, J.; Lu, W.; Lin, X.; Zhang, Y.; Tian, B.; Yang, H.; He, H. PEG−PLGA copolymers: Their structure and structure-influenced drug delivery applications. *J. Controlled Release* **2014**, *183*, 77−86.
(18) Lepeltier, E.; Bourgaux, C.; Couvreur, P. Nanoprecipitation and the "Ouzo effect": Application to drug delivery devices. *Adv. Drug Delivery* **2014**, *71*, 86−97, DOI: 10.1016/j.addr.2013.12.009.
(19) Beck-Broichsitter, M.; Rytting, E.; Lebhardt, T.; Wang, X.; Kissel, T. Preparation of nanoparticles by solvent displacement for drug delivery: A shift in the "ouzo region" upon drug loading. *Eur. J. Pharm. Sci.* **2010**, *41* (2), 244−253.
(20) Sternling, C. V.; Scriven, L. E. Interfacial turbulence: Hydrodynamic instability and the marangoni effect. *AIChE J.* **1959**, *5* (4), 514−523, DOI: 10.1002/aic.690050421.
(21) Barreras-Urbina, C. G.; Ramírez-Wong, B.; López-Ahumada, G. A.; Burruel-Ibarra, S. E.; Martínez-Cruz, O.; Tapia-Hernández, J. A.; Félix, F. R. Nano- and Micro-Particles by Nanoprecipitation: Possible Application in the Food and Agricultural Industries. *Int. J. Food Prop.* **2016**, *19* (9), 1912−1923, DOI: 10.1080/10942912.2015.1089279.
(22) Bilati, U.; Allémann, E.; Doelker, E. Development of a nanoprecipitation method intended for the entrapment of hydrophilic drugs into nanoparticles. *Eur. J. Pharm. Sci.* **2005**, *24*, 67−75, DOI: 10.1016/j.ejps.2004.09.011.
(23) Langer, R.; Folkman, J. Polymers for the sustained release of proteins and other macromolecules. *Nature* **1976**, *263* (5580), 797−800.
(24) Yadav, K. S.; Sawant, K. K. Modified nanoprecipitation method for preparation of cytarabine-loaded PLGA nanoparticles. *AAPS PharmSciTech* **2010**, *11*, 1456−1465, DOI: 10.1208/s12249-010-9519-4.
(25) Morales-Cruz, M.; Flores-Fernández, G. M.; Morales-Cruz, M.; Orellano, E. A.; Rodriguez-Martinez, J. A.; Ruiz, M.; Griebenow, K. Two-step nanoprecipitation for the production of protein-loaded PLGA nanospheres. *Results Pharma Sci.* **2012**, *2*, 79−85.
(26) Tarhini, M.; Benlyamani, I.; Hamdani, S.; Agusti, G.; Fessi, H.; Greige-Gerges, H.; Bentaher, A.; Elaissari, A. Protein-Based Nanoparticle Preparation via Nanoprecipitation Method. *Materials* **2018**, *11*, No. 394, DOI: 10.3390/ma11030394.
(27) Chen, B.; Xiang, S.; Qian, G. Metal−Organic Frameworks with Functional Pores for Recognition of Small Molecules. *Acc. Chem. Res.* **2010**, *43* (8), 1115−1124.
(28) Lohe, M. R.; Gedrich, K.; Freudenberg, T.; Kockrick, E.; Dellmann, T.; Kaskel, S. Heating and separation using nanomagnet-functionalized metal−organic frameworks. *Chem. Commun.* **2011**, *47* (11), 3075−3077, DOI: 10.1039/c0cc05278g.
(29) Liu, B. Metal−organic framework-based devices: separation and sensors. *J. Mater. Chem.* **2012**, *22* (20), 10094−10101, DOI: 10.1039/c2jm15827b.
(30) Zhou, H.-C.; Long, J. R.; Yaghi, O. M. Introduction to Metal−Organic Frameworks. *Chem. Rev.* **2012**, *112* (2), 673−674, DOI: 10.1021/cr300014x.
(31) Chen, B.; Yang, Z.; Zhu, Y.; Xia, Y. Zeolitic imidazolate framework materials: recent progress in synthesis and applications. *J. Mater. Chem. A* **2014**, *2* (40), 16811−16831, DOI: 10.1039/C4TA02984D.
(32) Mittal, A.; Gandhi, S.; Roy, I. Mechanistic interaction studies of synthesized ZIF-8 nanoparticles with bovine serum albumin using spectroscopic and molecular docking approaches. *Sci. Rep.* **2022**, *12* (1), No. 10331.
(33) Lyu, F.; Zhang, Y.; Zare, R. N.; Ge, J.; Liu, Z. One-pot synthesis of protein-embedded metal-organic frameworks with enhanced biological activities. *Nano Lett.* **2014**, *14*, 5761−5765, DOI: 10.1021/nl5026419.
(34) Wang, X.; He, L.; Sumner, J.; Qian, S.; Zhang, Q.; O'Neill, H.; Mao, Y.; Chen, C.; Al-Enizi, A. M.; Nafady, A.; Ma, S. Spatially confined protein assembly in hierarchical mesoporous metal-organic framework. *Nat. Commun.* **2023**, *14* (1), No. 973, DOI: 10.1038/s41467-023-36533-w.

(35) Deng, H.; Grunder, S.; Cordova, K. E.; Valente, C.; Furukawa, H.; Hmadeh, M.; Gándara, F.; Whalley, A. C.; Liu, Z.; Asahina, S.; et al. Large-Pore Apertures in a Series of Metal-Organic Frameworks. *Science* **2012**, *336* (6084), 1018−1023, DOI: 10.1126/science.1220131.
(36) Xia, H.; Li, N.; Huang, W.; Song, Y.; Jiang, Y. Enzymatic Cascade Reactions Mediated by Highly Efficient Biomimetic Quasi Metal−Organic Frameworks. *ACS Appl. Mater. Interfaces* **2021**, *13* (19), 22240−22253.
(37) Klermund, L.; Castiglione, K. Polymersomes as nanoreactors for preparative biocatalytic applications: current challenges and future perspectives. *Bioprocess Biosyst. Eng.* **2018**, *41* (9), 1233−1246.
(38) Furukawa, H.; Cordova, K. E.; O'Keeffe, M.; Yaghi, O. M. The Chemistry and Applications of Metal-Organic Frameworks. *Science* **2013**, *341* (6149), No. 1230444.
(39) Xia, H.; Zhong, X.; Li, Z.; Jiang, Y. Palladium-mediated hybrid biocatalysts with enhanced enzymatic catalytic performance via allosteric effects. *J. Colloid Interface Sci.* **2019**, *533*, 1−8.
(40) Semino, R.; Moreton, J. C.; Ramsahye, N. A.; Cohen, S. M.; Maurin, G. Understanding the origins of metal−organic framework/polymer compatibility. *Chem. Sci.* **2018**, *9* (2), 315−324, DOI: 10.1039/C7SC04152G.
(41) Cai, C.; Bakowsky, U.; Rytting, E.; Schaper, A. K.; Kissel, T. Charged nanoparticles as protein delivery systems: A feasibility study using lysozyme as model protein. *Eur. J. Pharm. Biopharm.* **2008**, *69* (1), 31−42.
(42) Rivas, C. J. M.; Tarhini, M.; Badri, W.; Miladi, K.; Greige-Gerges, H.; Nazari, Q. A.; Rodríguez, S. A. G.; Román, R. Á.; Fessi, H.; Elaissari, A. Nanoprecipitation process: From encapsulation to drug delivery. *Int. J. Pharm.* **2017**, *532* (1), 66−81.
(43) Yang, G.; Liu, Y.; Jin, S.; Hui, Y.; Wang, X.; Xu, L.; Chen, D.; Weitz, D.; Zhao, C.-X. Phase separation-induced nanoprecipitation for making polymer nanoparticles with high drug loading. *Aggregate* **2023**, *4*, No. e314.
(44) Zhang, X. Y.; Zhang, P. Y. Polymersomes in Nanomedicine - A Review. *Curr. Nanosci.* **2017**, *13* (2), 124−129.
(45) Makadia, H. K.; Siegel, S. J. Poly Lactic-co-Glycolic Acid (PLGA) as Biodegradable Controlled Drug Delivery Carrier. *Polymers* **2011**, *3*, 1377−1397, DOI: 10.3390/polym3031377.
(46) Neupane, S.; Patnode, K.; Li, H.; Baryeh, K.; Liu, G.; Hu, J.; Chen, B.; Pan, Y.; Yang, Z. Enhancing Enzyme Immobilization on Carbon Nanotubes via Metal−Organic Frameworks for Large-Substrate Biocatalysis. *ACS Appl. Mater. Interfaces* **2019**, *11* (12), 12133−12141.
(47) Chitemere, R. P.; Stafslien, S.; Rasulev, B.; Webster, D. C.; Quadir, M. Soysome: A Surfactant-Free, Fully Biobased, Self-Assembled Platform for Nanoscale Drug Delivery Applications. *ACS Appl. Bio Mater.* **2018**, *1* (6), 1830−1841.
(48) Bansal, K.; Webster, D.; Quadir, M. Self-Assembled Nanostructures from Amphiphilic Sucrose-Soyates for Solubilizing Hydrophobic Guest Molecules. *Langmuir* **2022**, *38* (6), 2066−2075.
(49) Smith, P. K.; Krohn, R. I.; Hermanson, G. T.; Mallia, A. K.; Gartner, F. H.; Provenzano, M. D.; Fujimoto, E. K.; Goeke, N. M.; Olson, B. J.; Klenk, D. C. Measurement of protein using bicinchoninic acid. *Anal. Biochem.* **1985**, *150* (1), 76−85.
(50) Watcharadulyarat, N.; Rattanatayarom, M.; Ruangsawasdi, N.; Patikarnmonthon, N. PEG−PLGA nanoparticles for encapsulating ciprofloxacin. *Sci. Rep.* **2023**, *13* (1), No. 266.
(51) Mansor, M. H.; Najberg, M.; Contini, A.; Alvarez-Lorenzo, C.; Garcion, E.; Jérôme, C.; Boury, F. Development of a non-toxic and non-denaturing formulation process for encapsulation of SDF-1α into PLGA/PEG-PLGA nanoparticles to achieve sustained release. *Eur. J. Pharm. Biopharm.* **2018**, *125*, 38−50, DOI: 10.1016/j.ejpb.2017.12.020.
(52) Khan, M. R. H.; Hazra, R. S.; Nair, G.; Mohammad, J.; Jiang, L.; Reindl, K.; Jawed, M. K.; Ganai, S.; Quadir, M. Cellulose nanofibers as Scaffold-forming materials for thin film drug delivery systems. *Int. J. Pharm.* **2022**, *627*, No. 122189.
(53) Schneider, N.; Weigel, I.; Werkmeister, K.; Pischetsrieder, M. Development and Validation of an Enzyme-Linked Immunosorbent Assay (ELISA) for Quantification of Lysozyme in Cheese. *J. Agric. Food Chem.* **2010**, *58* (1), 76−81.
(54) Pan, Y.; Li, Q.; Li, H.; Lenertz, M.; Jordahl, D.; Armstrong, Z.; Chen, B.; Yang, Z. Maximizing the applicability of continuous wave (CW) Electron Paramagnetic Resonance (EPR): what more can we do after a century? *J. Magn. Reson. Open* **2022**, *10−11*, No. 100060.
(55) Shi, P.; Luo, S.; Voit, B.; Appelhans, D.; Zan, X. A facile and efficient strategy to encapsulate the model basic protein lysozyme into porous CaCO3. *J. Mater. Chem. B* **2018**, *6* (25), 4205−4215, DOI: 10.1039/C8TB00312B.
(56) Shugar, D. The measurement of lysozyme activity and the ultra-violet inactivation of lysozyme. *Biochim. Biophys. Acta* **1952**, *8*, 302−309.
(57) Meng, F. T.; Ma, G. H.; Qiu, W.; Su, Z. G. W/O/W double emulsion technique using ethyl acetate as organic solvent: effects of its diffusion rate on the characteristics of microparticles. *J. Controlled Release* **2003**, *91*, 407−416, DOI: 10.1016/s0168-3659(03)00273-6.
(58) Lee, Y. C.; Yang, D. Determination of lysozyme activities in a microplate format. *Anal. Biochem.* **2002**, *310* (2), 223−224.
(59) Yadav, H.; Khan, M. R. H.; Quadir, M.; Rusch, K. A.; Mondal, P. P.; Orr, M.; Xu, E. G.; Iskander, S. M. Cutting Boards: An Overlooked Source of Microplastics in Human Food? *Environ. Sci. Technol.* **2023**, *57* (22), 8225−8235.
(60) Almoustafa, H. A.; Alshawsh, M. A.; Chik, Z. Technical aspects of preparing PEG-PLGA nanoparticles as carrier for chemotherapeutic agents by nanoprecipitation method. *Int. J. Pharm.* **2017**, *533* (1), 275−284, DOI: 10.1016/j.ijpharm.2017.09.054.
(61) Mares, A. G.; Pacassoni, G.; Marti, J. S.; Pujals, S.; Albertazzi, L. Formulation of tunable size PLGA-PEG nanoparticles for drug delivery using microfluidic technology. *PLoS One* **2021**, *16*, No. e0251821, DOI: 10.1371/journal.pone.0251821.
(62) Lababidi, N.; Sigal, V.; Koenneke, A.; Schwarzkopf, K.; Manz, A.; Schneider, M. Microfluidics as tool to prepare size-tunable PLGA nanoparticles with high curcumin encapsulation for efficient mucus penetration. *Beilstein J. Nanotechnol.* **2019**, *10*, 2280−2293, DOI: 10.3762/bjnano.10.220.
(63) Raval, N.; Maheshwari, R.; Kalyane, D.; Youngren-Ortiz, S. R.; Chougule, M. B.; Tekade, R. K. Importance of Physicochemical Characterization of Nanoparticles in Pharmaceutical Product Development. In *Basic Fundamentals of Drug Delivery*; Tekade, R. K., Ed.; Academic Press, 2019; Chapter 10, pp 369−400.
(64) Russell, B. A.; Jachimska, B.; Komorek, P.; Mulheran, P. A.; Chen, Y. Lysozyme encapsulated gold nanoclusters: effects of cluster synthesis on natural protein characteristics. *Phys. Chem. Chem. Phys.* **2017**, *19* (10), 7228−7235, DOI: 10.1039/C7CP00540G.
(65) Valstar, A.; Brown, W.; Almgren, M. The Lysozyme−Sodium Dodecyl Sulfate System Studied by Dynamic and Static Light Scattering. *Langmuir* **1999**, *15* (7), 2366−2374.
(66) Li, D.; Sun, H.; Ding, J.; Tang, Z.; Zhang, Y.; Xu, W.; Zhuang, X.; Chen, X. Polymeric topology and composition constrained polyether−polyester micelles for directional antitumor drug delivery. *Acta Biomater.* **2013**, *9* (11), 8875−8884.
(67) Cui, J.; Zhou, J.; Huang, L.; Jing, J.; Wang, N.; Wang, L. Curcumin encapsulation and protection based on lysozyme nanoparticles. *Food Sci. Nutr.* **2019**, *7*, 2702−2707, DOI: 10.1002/fsn3.1129.
(68) Yahia, M.; Phan Le, Q. N.; Ismail, N.; Essalhi, M.; Sundman, O.; Rahimpour, A.; Dal-Cin, M. M.; Tavajohi, N. Effect of incorporating different ZIF-8 crystal sizes in the polymer of intrinsic microporosity, PIM-1, for CO2/CH4 separation. *Microporous Mesoporous Mater.* **2021**, *312*, No. 110761.
(69) Win, K. Y.; Feng, S. S. Effects of particle size and surface coating on cellular uptake of polymeric nanoparticles for oral delivery of anticancer drugs. *Biomaterials* **2005**, *26*, 2713−2722, DOI: 10.1016/j.biomaterials.2004.07.050.
(70) Devasvaran, K.; Jairaman, S.; Yahaya, N. A.; Jaganath, I. B. S.; Khung, Y. L.; Lim, V.; Ngalim, S. H. PEG-b-PLGA Nanoparticles

Loaded with Geraniin from Phyllanthus Watsonii Extract as a Phytochemical Delivery Model. *Appl. Sci.* **2020**, *10*, No. 4891, DOI: 10.3390/app10144891.
(71) Liu, J.; Xu, H.; Tang, X.; Xu, J.; Jin, Z.; Li, H.; Wang, S.; Gou, J.; Jin, X. Simple and tunable surface coatings via polydopamine for modulating pharmacokinetics, cell uptake and biodistribution of polymeric nanoparticles. *RSC Adv.* **2017**, *7* (26), 15864−15876, DOI: 10.1039/C7RA01354J.
(72) Gayathri, S.; Arunkumar, P.; Bose, R.; Alfantazi, A.; Han, J. H. A hexagonal 2D ZIF-Co-L variant: Unusual role of graphene oxide on the water-regulated morphology of ZIF hybrid and their derived Co@N-doped carbon electrocatalyst for hydrogen evolution reaction. *Chem. Eng. J.* **2021**, *426*, No. 131270.
(73) Wais, U.; Jackson, A. W.; He, T.; Zhang, H. Nanoformulation and encapsulation approaches for poorly water-soluble drug nanoparticles. *Nanoscale* **2016**, *8* (4), 1746−1769, DOI: 10.1039/C5NR07161E.
(74) Hansen, J.; Ely, K.; Horsley, D.; Herron, J.; Hlady, V.; Andrade, J. D. The adsorption of lysozymes: A model system. *Makromol. Chem., Macromol. Symp.* **1988**, *17* (1), 135−154, DOI: 10.1002/masy.19880170110.
(75) Hazra, R. S.; Dutta, D.; Mamnoon, B.; Nair, G.; Knight, A.; Mallik, S.; Ganai, S.; Reindl, K.; Jiang, L.; Quadir, M. Polymeric Composite Matrix with High Biobased Content as Pharmaceutically Relevant Molecular Encapsulation and Release Platform. *ACS Appl. Mater. Interfaces* **2021**, *13* (34), 40229−40248.
(76) Justus, C. R.; Dong, L.; Yang, L. V. Acidic tumor microenvironment and pH-sensing G protein-coupled receptors. *Front. Physiol.* **2013**, *4*, No. 70722, DOI: 10.3389/fphys.2013.00354.
(77) Lin, B.; Chen, H.; Liang, D.; Lin, W.; Qi, X.; Liu, H.; Deng, X. Acidic pH and High-H2O2 Dual Tumor Microenvironment-Responsive Nanocatalytic Graphene Oxide for Cancer Selective Therapy and Recognition. *ACS Appl. Mater. Interfaces* **2019**, *11* (12), 11157−11166.
(78) Diwan, M.; Park, T. G. Pegylation enhances protein stability during encapsulation in PLGA microspheres. *J. Controlled Release* **2001**, *73*, 233−244, DOI: 10.1016/s0168-3659(01)00292-9.
(79) Milacic, V.; Schwendeman, S. P. Lysozyme release and polymer erosion behavior of injectable implants prepared from PLGA-PEG block copolymers and PLGA/PLGA-PEG blends. *Pharm. Res.* **2014**, *31*, 436−448, DOI: 10.1007/s11095-013-1173-6.
(80) Luan, X.; Bodmeier, R. Modification of the tri-phasic drug release pattern of leuprolide acetate-loaded poly(lactide-co-glycolide) microparticles. *Eur. J. Pharm. Biopharm.* **2006**, *63*, 205−214, DOI: 10.1016/j.ejpb.2005.12.010.
(81) Zolnik, B. S.; Burgess, D. J. Effect of acidic pH on PLGA microsphere degradation and release. *J. Controlled Release* **2007**, *122* (3), 338−344.
(82) Truong, P. L.; Thao, N. T. T.; Le Huyen, H. T.; Nguyen, T. H. Ultrasensitive Detection of Lysozyme upon Conformational Change of DNA Duplex. *J. Nanomater.* **2022**, *2022*, No. 1107081.
(83) Sakamoto, S. A.-O. X.; Putalun, W.; Vimolmangkang, S.; Phoolcharoen, W.; Shoyama, Y.; Tanaka, H.; Morimoto, S. Enzyme-linked immunosorbent assay for the quantitative/qualitative analysis of plant secondary metabolites. *J. Nat. Med.* **2018**, *72*, 32−42, DOI: 10.1007/s11418-017-1144-z.
(84) Greenfield, N. J. Using circular dichroism spectra to estimate protein secondary structure. *Nat. Protoc.* **2006**, *1* (6), 2876−2890.
(85) Sheng, L.; Wang, J.; Huang, M.; Xu, Q.; Ma, M. The changes of secondary structures and properties of lysozyme along with the egg storage. *Int. J. Biol. Macromol.* **2016**, *92*, 600−606, DOI: 10.1016/j.ijbiomac.2016.07.068.
(86) Temboot, P.; Usman, F.; Ul-Haq, Z.; Khalil, R.; Srichana, T. Biomolecular interactions of amphotericin B nanomicelles with serum albumins: A combined biophysical and molecular docking approach. *Spectrochim. Acta, Part A* **2018**, *205*, 442−456, DOI: 10.1016/j.saa.2018.07.057.
(87) Wang, Y. X.; Li, L.; Sheng, L. J.; Song, G. W.; Xu, Z. S. Spectroscopic study on the inherent binding information of cationic perfluorinated surfactant with bovine serum albumin. *J. Fluorine Chem.* **2011**, *132* (7), 489−494.
(88) Lawrence, G.; Baskar, A. V.; El-Newehy, M. H.; Cha, W. S.; Al-Deyab, S. S.; Vinu, A. Quick high-temperature hydrothermal synthesis of mesoporous materials with 3D cubic structure for the adsorption of lysozyme. *Sci. Technol. Adv. Mater.* **2015**, *16* (2), No. 024806.
(89) Kumar, P.; Bansal, V.; Paul, A. K.; Bharadwaj, L. M.; Deep, A.; Kim, K.-H. Biological applications of zinc imidazole framework through protein encapsulation. *Appl. Nanosci.* **2016**, *6* (7), 951−957.
(90) Todd, A. P.; Cong, J.; Levinthal, F.; Levinthal, C.; Hubell, W. L. Site-directed mutagenesis of colicin E1 provides specific attachment sites for spin labels whose spectra are sensitive to local conformation. *Proteins: Struct., Funct., Bioinf.* **1989**, *6* (3), 294−305, DOI: 10.1002/prot.340060312.
(91) Fleissner, M. R.; Brustad, E. M.; Kálai, T.; Altenbach, C.; Cascio, D.; Peters, F. B.; Hideg, K.; Peuker, S.; Schultz, P. G.; Hubbell, W. L. Site-directed spin labeling of a genetically encoded unnatural amino acid. *Proc. Natl. Acad. Sci. U.S.A.* **2009**, *106* (51), 21637−21642, DOI: 10.1073/pnas.0912009106.
(92) Pan, Y.; Li, H.; Farmakes, J.; Xiao, F.; Chen, B.; Ma, S.; Yang, Z. How Do Enzymes Orient When Trapped on Metal−Organic Framework (MOF) Surfaces? *J. Am. Chem. Soc.* **2018**, *140* (47), 16032−16036.
(93) Hubbell, W. L.; López, C. J.; Altenbach, C.; Yang, Z. Technological advances in site-directed spin labeling of proteins. *Curr. Opin. Struct. Biol.* **2013**, *23* (5), 725−733.
(94) Hubbell, W. L.; Altenbach, C. Investigation of structure and dynamics in membrane proteins using site-directed spin labeling. *Curr. Opin. Struct. Biol.* **1994**, *4* (4), 566−573.
(95) Pan, Y.; Li, H.; Li, Q.; Lenertz, M.; Zhu, X.; Chen, B.; Yang, Z. Site-directed spin labeling-electron paramagnetic resonance spectroscopy in biocatalysis: Enzyme orientation and dynamics in nanoscale confinement. *Chem. Catal.* **2021**, *1* (1), 207−231.
(96) Pan, Y.; Li, H.; Li, Q.; Lenertz, M.; Schuster, I.; Jordahl, D.; Zhu, X.; Chen, B.; Yang, Z. Protocol for resolving enzyme orientation and dynamics in advanced porous materials via SDSL-EPR. *STAR Protoc.* **2021**, *2* (3), No. 100676.
(97) Khorshidian, N.; Khanniri, E.; Koushki, M. R.; Sohrabvandi, S.; Yousefi, M. An Overview of Antimicrobial Activity of Lysozyme and Its Functionality in Cheese. *Front. Nutr.* **2022**, *9*, No. 833618, DOI: 10.3389/fnut.2022.833618.
(98) Gutiérrez, D.; Briers, Y. Lysins breaking down the walls of Gram-negative bacteria, no longer a no-go. *Curr. Opin. Biotechnol.* **2021**, *68*, 15−22, DOI: 10.1016/j.copbio.2020.08.014.
(99) Primo, E. D.; Otero, L. H.; Ruiz, F.; Klinke, S.; Giordano, W. The disruptive effect of lysozyme on the bacterial cell wall explored by an in-silico structural outlook. *Biochem. Mol. Biol. Educ.* **2018**, *46*, 83−90, DOI: 10.1002/bmb.21092.
(100) Swed, A.; Cordonnier, T.; Fleury, F.; Boury, F. Protein Encapsulation into PLGA Nanoparticles by a Novel PhaseSeparation Method Using Non-Toxic Solvents. *J. Nanomed. Nanotechnol.* **2014**, *5*, 1−8, DOI: 10.4172/2157-7439.1000241.
(101) Semete, B.; Booysen, L.; Lemmer, Y.; Kalombo, L.; Katata, L.; Verschoor, J.; Swai, H. S. In vivo evaluation of the biodistribution and safety of PLGA nanoparticles as drug delivery systems. *Nanomed.: Nanotechnol. Biol. Med.* **2010**, *6*, 662−671, DOI: 10.1016/j.nano.2010.02.002.
(102) Hoop, M.; Walde, C. F.; Riccò, R.; Mushtaq, F.; Terzopoulou, A.; Chen, X.-Z.; deMello, A. J.; Doonan, C. J.; Falcaro, P.; Nelson, B. J.; et al. Biocompatibility characteristics of the metal organic framework ZIF-8 for therapeutical applications. *Appl. Mater. Today* **2018**, *11*, 13−21.
(103) de Almeida, M. S.; Susnik, E.; Drasler, B.; Taladriz-Blanco, P.; Petri-Fink, A.; Rothen-Rutishauser, B. Understanding nanoparticle endocytosis to improve targeting strategies in nanomedicine. *Chem. Soc. Rev.* **2021**, *50* (9), 5397−5434, DOI: 10.1039/D0CS01127D.
(104) Wojnilowicz, M.; Glab, A.; Bertucci, A.; Caruso, F.; Cavalieri, F. Super-resolution Imaging of Proton Sponge-Triggered Rupture of

Endosomes and Cytosolic Release of Small Interfering RNA. *ACS Nano* **2019**, *13*, 187−202, DOI: 10.1021/acsnano.8b05151.
(105) Vermeulen, L. M. P.; De Smedt, S. C.; Remaut, K.; Braeckmans, K. The proton sponge hypothesis: Fable or fact? *Eur. J. Pharm. Biopharm.* **2018**, *129*, 184−190.
(106) Cao, L.-B.; Zeng, S.; Zhao, W. Highly Stable PEGylated Poly(lactic-co-glycolic acid) (PLGA) Nanoparticles for the Effective Delivery of Docetaxel in Prostate Cancers. *Nanoscale Res. Lett.* **2016**, *11* (1), No. 305, DOI: 10.1186/s11671-016-1509-3.
(107) Devrim, B.; Kara, A.; Vural, İ.; Bozkır, A. Lysozyme-loaded lipid-polymer hybrid nanoparticles: preparation, characterization and colloidal stability evaluation. *Drug Dev. Ind. Pharm.* **2016**, *42* (11), 1865−1876, DOI: 10.1080/03639045.2016.1180392.
(108) Zhao, H.; Gong, L.; Wu, H.; Liu, C.; Liu, Y.; Xiao, C.; Liu, C.; Chen, L.; Jin, M.; Gao, Z.; et al. Development of Novel Paclitaxel-Loaded ZIF-8 Metal-Organic Framework Nanoparticles Modified with Peptide Dimers and an Evaluation of Its Inhibitory Effect against Prostate Cancer Cells. *Pharmaceutics* **2023**, *15*, No. 1874, DOI: 10.3390/pharmaceutics15071874.
(109) Minko, T.; Dharap, S.; Pakunlu, R.; Wang, Y. Molecular targeting of drug delivery systems to cancer. *Curr. Drug Targets* **2004**, *5*, 389−406, DOI: 10.2174/1389450043345443.